Model-based Microfluidic Device Design for Refreshable Braille and Tactile Graphics

by

Alexander Russomanno

A dissertation submitted in partial fulfillment
of the requirements for the degree of
Doctor of Philosophy
(Mechanical Engineering)
in the University of Michigan
2017

Doctoral Committee:

Associate Professor Brent Gillespie, Chair
Professor Mark Burns
Professor Karl Grosh
Associate Professor Sile O'Modhrain

Alexander Russomanno

arussoma@umich.edu

ORCID iD: 0000-0002-5832-4564

This dissertation is dedicated to my mom and dad,

for their encouragement and support,

and for all the LEGO and K'NEX.

ACKNOWLEDGEMENTS

I would first like to thank the Department of Mechanical Engineering and the National Science Foundation for their financial support under a departmental fellowship and Grant IIS 1319922, respectively. The opportunity to conduct research at the University of Michigan has been an incredible honor.

I owe a tremendous amount of gratitude to everyone that has worked with me in the HaptiX Lab over the course of my research. They listened to practice presentations, helped me design and troubleshoot experimental setups, and provided essential feedback on research.

I am extremely grateful to my advisor Brent Gillespie for his support in both my personal and professional life. I learned early on that Brent was a great champion of his students. He devoted generous amounts of time, often at odd hours of the day I might add, to helping everyone in his lab write papers, prepare presentations, and conduct research. Under his guidance, I became a better scholar and person. I also want to thank Brent and his family, Mary-Anne, Booker, and Lincoln, for being so welcoming over the years. I've greatly enjoyed getting to know them and look forward to staying in touch in the future.

I'm also thankful for all the wonderful people I've met in Ann Arbor. The friendships I've made have been incredibly fulfilling.

Finally, I want to thank my family for their support. They have lent much-needed guidance and motivation throughout my life and for that, I am eternally grateful.

TABLE OF CONTENTS

LIST OF FIGURES

Figure

LIST OF TABLES

Table

ABSTRACT

Model-based Microfluidic Device Design
for Refreshable Braille and Tactile Graphics

by

Alexander Russomanno

Chair: Brent Gillespie

A low-cost and reliable technology to support electronic braille displays would significantly increase access to digital media for blind braille readers. Even better, a full-page dense array of refreshable braille-sized dots could be used to display both braille and tactile graphics—a feat not achievable by existing technologies. The work in this dissertation is two-pronged. First, a perceptual study was carried out that motivates and guides the design of a full-page display. Second, a model-based design approach is adopted to develop microfluidic technology to overcome critical challenges in creating a full-page display.

A full-page display is made up of thousands of densely-packed dots, each requiring a dedicated actuator. Some design solutions have been proposed which reduce the number of actuators by using a small array that travels along with the reading finger (think: braille cell on a computer mouse), eliminating sliding contact as a consequence. Based on this consideration, a perceptual study was carried out that informs the design of a full-page display. The study quantifies the reduction in braille character recognition imposed by display designs that reduce sliding contact.

Microfluidic technology is employed to fabricate tiny channels and chambers in soft silicone that address and raise braille-sized bubble features on a surface. The challenge associated with controlling many individual fluidic features is met by integrating digital fluidic logic networks with the actuators. Each dot is addressed by the combination of a fluid actuator and a basic fluidic memory unit. A memory unit stores high or low pressure as a binary signal that determines whether its corresponding actuator is up or down. Crucially, memory units can be cascaded so the output of one controls the input of another. Pressure-encoded 1s and 0s can be shifted along cascaded memory units, thereby reducing the required number of external valves. To ensure that the design is sufficiently scalable and manufacturable to support the realization of a large dense array of pins at braille spacing, two performance criteria must be attained. The first is ensuring the memory units are cascadable. The second is controlling memory units at speeds suitable for refreshable braille. The work in this dissertation addresses these two performance criteria by developing models of digital fluidic circuits with particular attention to design parameters that affect circuit cascadability and speed.

CHAPTER I

Introduction

1.1 Motivation

The increased access to books afforded to blind people via e-publishing has given them long-sought independence for both recreational and educational reading. In most cases, blind readers access materials using text-to-speech output. For some content such as highly technical texts, music, and graphics, speech is not an appropriate access modality as it does not promote deep understanding. Therefore blind braille readers often prefer refreshable braille displays that electronically raise braille text on a surface. These displays are prohibitively expensive, due to the underlying technology used to raise braille dots, and are limited to a single line, making reading difficult and displaying tactile graphics impossible. The search is on, therefore, for a low-cost refreshable display that would go beyond current technologies and deliver graphical content as well as text in a full-page format.

The challenge of programmably raising thousands of braille-dot-sized features on a large surface is well-known. Solutions to the problem usually take one of the following forms:

1. The need for a large number of features is removed entirely by rendering touch sensations in a different way. For example, by actively modulating friction be-

tween the fingertip and a flat surface, devices are able to render tactile percepts like texture and feature edges.

2. The need for a large number of features is reduced by deploying a small array of active features that move with the finger. In one example, the array can be mounted on a position-sensing device, such as a computer mouse. The array of features raise up and down underneath the fingers as the mouse is moved.

3. A large number of active features are employed. The features are individually raised and controlled in a one-to-one mapping by electro-mechanical actuators or actuators based on other technologies.

In the first approach, forces are rendered uniformly across the entire finger in contact with the surface. Simple experiments reveal that haptic technologies that are unable to modulate the distribution of forces within the finger contact patch are not suitable for braille reading [79]. Therefore, these technologies are not able to render standard braille in their present form [72, 13]. In the second approach, the features only indent upward into the fingertip. Interaction with tactile content in this manner is much different than traditional braille reading, in which there is relative motion between reading surface and fingers as the hand moves. As will be discussed in this dissertation, displays that reduce size and cost by restricting the display to a small number of active features that move with the finger are likely to be less effective for braille reading. The third approach is perhaps the only viable option for achieving refreshable braille, but there are significant challenges related to its implementation.

This dissertation makes advancements toward addressing some of the challenges of the third approach described above, that is, creating a display with large number of active features.

In one thrust, a perceptual study is carried out that both motivate and provide guidelines for the design approach. In particular, the study addresses the importance

of sliding contact between features and the fingertip in braille reading. In another thrust, the dissertation focuses on the application of microfluidics for creating a refreshable braille display. Pressurized fluid (gas or liquid) from a common pressure source is used to raise bubble-like features on a surface. Using microfluidics, the source of fluid power can be separated from the point of actuation by a channel or pipe, enabling the features to be densely-packed. There are challenges to overcome in applying microfluidic technology to refreshable braille that relate to design requirements for braille. Specifically, features must (1) be individually controllable, (2) refresh quickly (on the order of 1 Hz), and (3) meet the force, deflection, and spacing (2.5 mm dot spacing) specifications for braille reading. The third challenge has been achieved in previous work [58], but the first two represent non-trivial design challenges not yet solved.

The difficultly of controlling a large array of tightly-packed fluidic features has limited the successful implementation of fluidic actuators for tactile displays. I propose that the complexity associated with controlling many individual fluidic features can be reduced by adding integrated fluidic logic networks in which each braille dot is addressed by the combination of a fluid actuator and a basic fluidic latching memory unit. The fluidic memory units store pressure as binary signals (high and low pressures) that can control the state of the actuator; individual actuators can then be addressed and controlled without dedicating a separate external pressure control feature, i.e. an electronic valve, to each actuator. The number of external electronic control valves can be reduced by several orders of magnitude. Similar to how the very-large-scale integration (VLSI) movement enabled mass scaling-down of electronic logic circuits to a single chip, fluidic logic networks might enable the large-scale integration of fluidic elements for the creation of a refreshable braille display.

A trade-off exists between the number of memory units implemented in a microfluidic control design and the refresh rate of a whole display. Bits of information,

encoded in high and low pressure, are passed in time along a line of memory units. After one "pressure bit" of information is applied, it takes time for pressure to settle before another bit can safely be applied. As the number of actuators (and corresponding memory units) increases, the refresh rate of the whole display decreases. Therefore, careful attention must be paid to the design of fluidic memory circuits to allow for sufficient whole-display refresh speeds.

With regards to these challenges, this dissertation advances the third enumerated solution from above, namely, the creation of a refreshable braille display with a large number of active features. The work motivates the selection of the design approach and focuses on the application of microfluidics for controlling a large number of features for a refreshable braille display. The contributes can be used applied to better design microfluidic actuators and circuits, with an emphasis on the control and timing of individual features for braille displays.

1.2 Contributions

This dissertation focuses on the development of a full-page dense-array tactile display suitable for displaying braille and tactile graphics using microfluidic technology. The work can be divided into two main areas: (1) tactile perception of refreshable braille and (2) the application of microfluidics for creating a refreshable braille and tactile graphics display. The following contributions will be presented in this dissertation:

1. **The Importance of Sliding Contact in Braille Letter Identification:** Restricting certain tactile cues during braille reading leads to decreased performance in a letter recognition task. Chapter II investigates the effects of various means for presenting braille characters to a reading finger on braille character recognition. The study finds that a lack of sliding contact between the fingertip

and the braille reading surface results in more errors and the number of errors increases as a function of presentation speed. The findings suggest that single cell displays which do not incorporate sliding contact are likely to be less effective for braille reading. They further motivate the creation of a full-page display in which exploration allows features to move across the fingertip.

2. **Relating Key Fluidic Valve Design Parameters to Cascadability of Fluidic Memory Circuits:** Cascading memory logic circuits for control of fluidic actuators requires fluidic valves, i.e. fluid transistors, with nonlinear gain and switching thresholds that give rise to two distinct logic levels. Previous work has demonstrated fluid transistors that achieve these behaviors, but these demonstrations have not been accompanied by parametric models. That is, no models have been introduced that attempt to combine key design elements, namely pre-load, area fraction, membrane stiffness, and circuit resistance, to predict valve behavior. This dissertation develops a model that describes fluidic valve behavior and as such, is a useful tool for designing microfluidic fluidic valves for cascadable logic circuits

3. **Relating Pressure-Dependent Resistance of Fluidic Valves to Fluidic Memory Circuit Timing:** Cascading memory logic circuits for control of fluidic actuators also leads to challenges with regard to control speed. While the performance of equivalent electronic memory circuits has been studied extensively, little work has been completed to characterize pneumatic circuits, which are governed by compressible flow and nonlinear, hysteretic fluidic valve behavior. A model of a pneumatic memory circuit that considers the dynamic behavior of the fluidic valve is presented in Chapter IV. The model is used to investigate how valve behavior affects signal propagation delays and thus circuit control speed.‘

1.3 Dissertation Overview

This dissertation focuses on the motivation for and creation of a full-page refreshable display suitable for rendering braille and tactile graphics.

Chapter II investigates the relationship between sliding contact between the braille and fingertip and braille letter recognition. Chapter III presents a parameterized model for fluidic valves that provides mechanistic explanations for features of cascadability in fluidic logic circuits. Chapter IV introduces a hybrid automaton model of a latching pneumatic memory circuit. The effect of the dynamic behavior of fluidic valves is explored, particularly as it effects the propagation delays of pressure signals in bistable pneumatic circuits. Finally, Chapter V summarizes the contributions of this dissertation and suggests future work.

CHAPTER II

Refreshing Refreshable Braille Displays

2.1 Introduction

There can be no doubt that blind people are now relatively self-sufficient when it comes to searching for and reading articles and books presented in electronic formats. However, the question arises as to whether their means of access (speech or braille) is optimal for promoting deep understanding of content. The preferred mode for reading electronic texts for most blind computer users is speech, because it is relatively inexpensive (or even free) when compared to braille and requires no additional hardware. However, as Varao Sousa et al [70] have demonstrated, listening to text being read is a fundamentally different experience from actively reading text for visual readers. They report that more active modes of reading (such as reading silently or reading aloud) lead to less mind-wandering and greater comprehension than when participants passively listened to text being read to them. It is likely that more active modes of processing text, e.g. through reading braille, would afford similar advantages for blind readers over passive reception via speech. For situations where comprehension of a text is a priority such as in educational settings, therefore, reading braille might be considered the optimal mode of information transmission. Moreover, for highly technical content such as mathematical and music notation, or for content of a highly spatial nature such as maps and charts, spoken descriptions

are a poor substitute for encountering the material directly through touch [26].

There are three factors that currently work against the use of braille as the primary reading modality for blind readers: 1) The cost of refreshable braille displays, which range from approximately $2,000 for a 18-character display to $50,000 for a half page of braille [1], 2) the decline in support for teaching braille to blind children and newly blind adults, which has resulted in a corresponding drop in levels of braille literacy [2], and 3) the increasing cost of producing hard copy braille books which has reduced the availability of recently published books in braille format, which in turn impacts the interest in and practice of braille reading, particularly for young readers.

For all of these reasons, the pressure to develop a novel approach to the design of refreshable braille displays is mounting [55],[2].

The fact that braille display technology has not changed significantly for 35 years is astonishing when considered alongside the continually shifting interaction paradigms of personal computing in general. In the years since the introduction of the first piezoelectric braille cell in 1979, we have witnessed the demise of the command line, the evolution of the Windows-Icons-Menus-Pointer (WIMP) interface and finally the birth of co-located input and output in the form of the touchscreen. All of this begs the question: What would it take to effect a similar revolution in the design of displays that support interaction with tactile content in the form of braille or tactile graphics? The first step, I argue, is to collect evidence regarding the haptic percepts that underpin the understanding of tactual information gathering. Gaining an appreciation for the contribution of such percepts might make it easier to design a braille display that can meet the needs of braille readers in todays electronic reading environment.

It has been clearly established that the understanding of braille is improved by active reading in which the hands pass over the surface of the braille text [43], [25]. There are two possible contributing factors: Firstly, that the continuous slip between

the skin and the surface provided by the motion across braille as it is read provides the continuous stimulation necessary to render the braille image, and secondly, that the proprioceptive cues provided as the hands move are also important in promoting the understanding of larger scale structure such as the spatial orientation of characters (see [43], Chapter 3 and Chapter 8.6). In this Chapter, the hypothesis that both of these components play a part in reading braille is tested. The study reported here systematically examines their relative contributions. If the hypothesis is supported, it would have implications for the design of refreshable braille displays.

2.2 Background

2.2.1 Research on Braille Reading

The study of how blind people read braille is by no means a new topic. Almost as soon as the code was invented and blind people became proficient at using braille, their sighted colleagues became interested in how it is possible to read via touch. Furthermore, educators wanted to know how best to teach braille to young and newly blind readers ([10], cited in [19]). In his extensive work on braille reading, Foulke determined that there are three primary reasons for studying the reading of braille: to study the processes that underpin the perception and cognition of braille, to determine the legibility of the braille code, and to study how reading performance changes as a function of varying the manner in which braille is displayed [19]. This last reason is of particular interest to anyone engaged in the search for a low-cost alternative to current display technologies, and it is to this category that the current work belongs.

Just as with Roman letters, the symbols in the braille code are displayed spatially. Unlike visual reading, however, the tactile system is not well equipped to process spatially distributed information the same way as vision. In fact, the question of whether braille readers construct words from the sequential processing of their

component symbols or whether, like visual readers, they can recognise words from their global shape (the so-called word superiority effect), is a matter that has been discussed at length [36], [43], (Chapter 4). As Millar points out, the sequential processing hypothesis suggests that tactile reading is a constructive process in line with aspects of haptic shape perception reported by Katz [34] and Lederman and Klatzky [38]. Global processing of word shapes, on the other hand, suggests a higher level of pattern matching more akin to vision. Millar suggests that experienced readers combine both approaches since familiar words are processed more quickly than words of the same length containing nonsense letters. Such findings support the hypothesis in that they point to a need for access to more than just the letter beneath the fingertip or, at the very least, to a need for the presence of some proprioceptive cues in reading that promote the spatial integration of letter sequences to form spatially extended words.

On the other hand, as [19] points out, tactile acuity, even on the fingertip, is much poorer than visual acuity. The two-point discrimination threshold is 2-4 mm in healthy adults [67], which is on the same order as the dot spacing. While the dots appear distinct visually, they may meld into shapes for the fingers. The 3×2 dot array that makes up a print braille character and 4×2 dot array that makes up a standard refreshable braille character are sized to fit the contact patch between the finger and the flat reading surface. But the tactual field of view is so much smaller than the visual field of view [19]. For these reasons, a pattern that can be resolved visually may not be resolvable through touch, so that the patterns that make up letters and symbols in braille are necessarily much simpler than letters of the visual alphabet. When matched in size and spatial resolution, braille characters are more easily distinguished through touch than are raised Roman letters presented to the fingertips [40]. Finally, because braille symbols are encountered individually and sequentially rather than in small groups as in vision, braille reading rates are much

slower, with typical reading rates for skilled adults of around 120 words per minute (WPM), compared to 300 WPM for visual reading (see [39] for an in-depth discussion of assessing braille reading speed).

2.2.1.1 Legibility of Braille Letters Under Different Display Conditions

As stated above, the motivation for the current study is to understand the relative contributions to braille reading of both relative motion between the fingertip and the braille reading surface (sliding) and the motion of the joints of the hand across the page (proprioception). While no prior work exists that addresses this question specifically for electronically displayed braille, two prior studies provide findings that are pertinent to the current experiment. Emerson Foulke's extensive body of work on braille was motivated, in large part, by a desire to find a way of improving performance in braille reading. His hypothesis was that, if the size of the braille cell could be increased to incorporate more dots, the code could be compressed to a greater degree than even grade II braille achieves in current usage. To this end, he carried out a series of studies to determine the manner in which the interaction between the fingertip and the braille reading surface predicted the efficiency of information pick-up. Using a modified version of an instrument called a tachistotactometer, which presented individual braille symbols by pressing them against the fingertip, Foulke and colleagues first sought to determine whether certain braille characters took longer for readers to identify than others [19]. Their hypothesis was that, if the correlation between the identification times for characters and their legibility thresholds (as determined by Nolan and Kederis [48]) was low, reading rates for braille might be determined more by the time spent identifying characters than by the time spent in registering the pattern of a stimulus.

In fact there was a low correlation between recognition time and legibility threshold, indicating that legibility of particular letters is not a predictor of braille reading

speed. Of significance for the current study, however, is Foulke's speculation that the manner of presentation of letters, i.e. the fact that they were pressed into the stationary fingertip, may have biased this result. He notes that this mode of presentation produces little deformation of the cutaneous tissue of the fingertip when compared to normal modes of braille reading. For this reason Foulke developed a second instrument that presented braille symbols on a tape that could be moved beneath the stationary fingertip under the control of a variable speed motor to restore sliding deformation of the fingertip and to simulate a range of reading rates. Kilpatrick (cited in [19]) used this tape apparatus to carry out a similar study of legibility thresholds, now incorporating sliding deformation. The threshold values he reported are somewhat lower than for studies with the tachistotactometer; however Foulke notes that this may be partly due to the fact that Kilpatrick did not control for the changes in time that the letters were available to be read as a function of changes in tape speed. Taken together, these studies point to an increase in performance when there is lateral motion between the fingertip and the braille reading surface, though they fail to provide a reliable measure of this effect.

A second body of work by Heller [25] sought to systematically examine the relative contributions of active and passive touch in braille reading performance. In his work, blindfolded sighted participants who had no prior experience with braille (unlike Foulke's skilled readers), were asked to match visual representations of braille characters and their Roman letter equivalents with tactile patterns presented to their fingertips. In the 'static' passive case, as with the tachistotactometer studies, braille symbols were pressed against the participant's stationary fingertip. This static case was used as a basis for comparison with three further cases in which the finger was static, but in which braille patterns were moved back and forth either vertically or horizontally in the plane of the braille reading surface at a constant speed. In a final passive case, the participant could request either vertical or horizontal presentation

(in an effort to restore some element of active control of presentation to the reader). In the active condition, participants could move their finger horizontally along a line of symbols, but were requested not to move vertically (trials where vertical movement was detected were dropped from their analysis). Their findings clearly supported their hypothesis, namely that active touch yielded superior performance when compared to all passive conditions, with static presentation of characters producing the poorest performance.

In an attempt to evaluate the efficacy of braille display configurations that could potentially use fewer braille cells (and hence cost less), the study reported here emulates aspects of both Heller's and Foulke's experimental design. A comparison is adopted between passive conditions from Heller's work, in which characters were presented either statically (Foulke's tachistotactometer study and Heller's passive static condition) or as patterns that moved across the stationary fingertip (Foulke's tape condition or Heller's passive horizontal condition). In addition, two further conditions were added in which the participant's reading hand was moved passively to restore some element of proprioceptive feedback, accompanied by either static presentation of braille under the moving fingertip or by the movement between the finger and the braille reading surface as the hand was drawn across it. In all cases the presentation of characters was timed, i.e. the interstimulus interval between presentation of successive characters was under computer control.

2.2.2 Refreshable Braille Technologies

The need to produce braille in a format that can be more easily stored, accessed and reproduced has long been recognised. Even as far back as 1916, a patent was filed for a spring-loaded refreshable display [8]. Since then, a surprising number of actuator technologies have been adapted to create refreshable braille including belt drives and tape drives [55]. Many more are actively being explored today, including

microfluidic technologies, electroactive polymers, and smart material actuators [55]. The diversity of these technologies, however, is not reflected in the array of devices currently available for purchase. In fact the piezo bimorph is still the only type of actuator to be found in today's commercialized braille displays. Importantly, many previous adaptations of actuator technology to the refreshable braille application have also required adaptations on the part of the braille reader. Adaptations to the manner in which braille is read can be enabling for certain actuator technologies, as is reviewed below. It is also quite likely that future technology developments will simultaneously explore adaptations to reading methods. Altering the reading method, however, might have adverse effects on the speed, comprehension, or pleasure of reading, and these effects have not been studied systematically.

2.2.3 Braille Reading Conditions

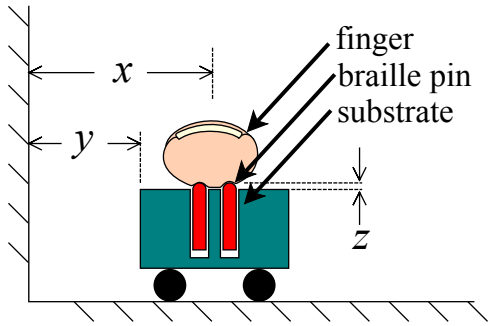

Figure 2.1: Simplified Schematic of a Refreshable Braille Display

An interesting issue that arises in today's paradigms for Human-Computer interaction is that of frames of reference for action. Think, for example, of the difference between magnifying text using eye glasses (worn on the head) as opposed to placing the text under a magnifying glass (mounted on a table). The effects on perception are profound, due to the availability of certain visual cues in one case but not the other. The cues in question are often those involving active, exploratory perceptual processes. A related design space exists for haptic and tactile displays, as is described

with the aid of Figure 2.1. In particular, relative motion may exist between the finger and a substrate holding pins or between the substrate and ground.

Figure 2.1 shows a pin protruding vertically a distance z from a substrate, as driven by an actuator that is embedded in the substrate and not shown. The substrate can be moved horizontally with displacement y relative to ground. Let x indicate the horizontal displacement of the reading finger relative to ground. Using the velocities $\dot{x}$ and $\dot{y}$, four conditions of interest are defined, as laid out in Figure 2.2. Across the rows in this table the substrate is either fixed ($\dot{y} = 0$) or moving to the right ($\dot{y} > 0$) while in the columns the finger is either fixed ($\dot{x} = 0$) or moving ($\dot{x} > 0$). For the lower right cell, $\dot{x} = \dot{y}$. Only the upper right cell in this table corresponds to normal braille reading (whether using embossed paper or a traditional refreshable braille display). But the other three cells present interesting cases, some of which correspond to proposed and to certain extent tested technologies, as is reviewed below. The names given to each of the cells correspond to these proposed technologies.

	Finger Fixed	Finger Moving
Substrate Fixed	**CLOCK** $\dot{x} = 0, \dot{y} = 0$ *Static* *Non-proprioceptive*	**LINE** $\dot{x} > 0, \dot{y} = 0$ *Sliding* *Proprioceptive*
Substrate Moving	**TAPE** $\dot{x} = 0, \dot{y} > 0$ *Sliding* *Non-proprioceptive*	**MOUSE** $\dot{x} = \dot{y} > 0$ *Static* *Proprioceptive*

Figure 2.2: A tabular arrangement of four conditions

Using Figure 2.2 as a framework, I briefly review a number of refreshable braille displays that may be unfamiliar to the reader as they either were not commercialized

or were unsuccessful as consumer products. I also include devices that were intended only for service as research apparatus. I am particularly interested in the modifications to reading methods imposed by these devices, expecting that future technologies will also explore modified reading methods.

As new technologies appear and their adaptations to refreshable braille are considered, the question naturally arises: what adaptations to the reading process might be undertaken by the braille reader? Perhaps adaptations to the braille code might even be considered that would be simple enough to learn.

Line Display: The standard means of reading braille is indicated with the label Line (short for Braille Line Display) in the upper right cell in Figure 2.2. The braille characters presented on an embossed page or on a single line refreshable braille display are stationary ($\dot{y} = 0$) while the fingers scan the page or line ($\dot{x} > 0$).

Tape Display: A family of devices that I refer to as Tape Displays uses a moving tape to carry braille dots past a stationary finger. Recall Folke's tape display apparatus, described earlier, which fed embossed paper tape past a stationary finger to study tradeoffs between reading speed and accuracy. A *refreshable* Tape Display features dots on the tape that can be selectively raised or lowered using actuators lying upstream from the reading finger. The IBM Wheeler Rubber Belt device dating from the 1950s featured a rubber belt loop with friction-gripped braille pins [9]. Grunwald's belt device (1966 [24]) featured a tape loop into which convex or concave protrusions could be punched by upstream actuators. The use of tape enables actuators to be more widely spaced, since adjacent dots need not be simultaneously punched.

Tactile Mouse: The response time of a pin driven by a piezo bimorph is quite short (on the order of a few tens of milliseconds). Yet the entire line in a commercial braille display is generally refreshed at one time and held in place while a person reads. Given the short response time and relatively compact actuators, the possibility exists

for braille characters to be refreshed right under the finger. The pins and actuators can be placed in a substrate whose motion is driven by finger or hand motion. I call this design the Tactile Mouse or Mouse for short, alluding to the use of a standard computer mouse as the substrate. The thumb and a few opposing fingers can drive motion while leaving the index finger free to read braille on the top of the mouse. A single commercial braille cell can be mounted on a movable substrate and the pins actuated according to the sensed substrate motion to create the impression of pins that are tied to ground. A computer mouse is the obvious platform, having position sensing already built-in.

Access to digital tactile graphics is perhaps a greater motivation for placing a braille cell or array of piezo bimorph-driven pins on a mouse than access to text. Similar to the case of braille, questions arise regarding ease of interpreting, comprehending, and recalling information contained in graphic images that are explored using pins that only press into the skin according to the location of the mouse rather than sliding across the skin. The perceptual processes at play in reading graphic images are certainly different than those operating during braille reading. However, we might expect that legibility of graphic elements or simplified graphic elements under conditions with and without lateral motion is somewhat related to the legibility of braille characters.

Several products have appeared on the market that incorporate piezo bimorph braille cells on a mouse, including the Virtouch (described in [73], now a discontinued product) and the Tactile Explorer Mouse (http://www.tactile-world.com/). Similar devices have been developed for research purposes [37].

Clock Display: Of course the option also exists for both the substrate and finger to remain stationary. That is, to present the braille characters in sequence under a finger that is not translating laterally. The braille pins simply present the characters in sequence under a fixed finger, making indentations into the finger that do not slide

laterally across the skin. This approach is often used to present the time on a braille reader, and thus I call it the Clock Display.

The refreshable braille devices discussed so far, based on various technologies to drive pins up and down, might be called *shape displays*. There are a number of emerging technologies that may be grouped roughly under the heading *surface haptics* that might also be adapted to create refreshable braille. Surface haptic technologies rely on various physical processes to modulate the force of friction as a finger is dragged across a flat surface [77] [5]. When the friction force is modulated as a function of position on the surface, the impression of a bump or hole can be produced [53]. However, these devices create tractions on the finger that are for the most part uniformly distributed. In particular, the distribution of traction forces within the contact surface of the finger is not programmable. Only a single bump or hole can be generated per finger contact; multiple bumps are not possible. Also note that the friction force always opposes motion and cannot be modulated under program control unless there is sliding contact between finger and flat surface. Thus surface haptic technologies would require changes to the braille code that remain to be explored.

In this chapter, I consider adaptations to the reading process required by braille displays in which there is no relative motion between the finger and substrate (the Clock and Mouse conditions) and displays in which the finger does not move (the Clock and Tape conditions). In the cases of the Mouse and Clock displays, cues associated with the sliding motion of the braille dots across the contact patch are missing. If the finger, hand, and arm are not advanced relative to ground then certain proprioceptive cues are missing, which is the case in the Clock and Tape conditions. The situation may be more complicated than the elimination of cues, however. For example, the ability of the reader to explore the text actively may be compromised. Whether the reader is in full control of the motion of text across the fingertips may have an effect on perception. The implications for reading tactile graphics also need

to be explored.

2.3 Mechanics of Fingertip Contact

A set of braille dots raised and lowered under a stationary finger deform the soft fingertip into a very different dynamic shape than a set of dots that slides across the skin. Determining the dynamic deformation patterns is a complex problem in contact mechanics involving an analysis of the soft fingertip touching the relatively hard braille reading surface. Here I only take a cursory look at this contact mechanics problem, with an aim to describe distinctions in the mechanical stimuli delivered to the mechanoreceptors by a static indentation versus a sliding indentation.

First note that the contact surface is not necessarily a connected surface; rather it is broken up into several disjoint contact patches. The soft skin will conform to the top rounded surface of each pin that is raised relative to the flat substrate, making a dome-shaped contact patch at each pin. But because the skin is not completely fluid, it will not conform to the sharp circular interface between each pin and substrate. Thus a gap will develop between the dome-shaped patch of skin in contact with a pin and a surrounding flat annular surface in contact with the substrate. Between the contact patches, the skin takes on a smooth shape that is governed by the mechanics of the skin and fingertip pulp. On the left in Figure 2.3, a photograph is shown, taken through a glass plate of a person reading braille embossed on transparent film. Contact surfaces almost the size of the fingertip are apparent under both index fingers. The photograph on the right in Figure 2.3 highlights the disconnected contact patch for a single fingertip. This image was created by inking a fingertip before touching the same braille-embossed transparent film with a light touch typical of braille reading. Each of the braille dots are inked, but a gap exists between the dots and the inked area of the substrate.

Naturally, the contact surface changes rapidly as a braille character is read. In

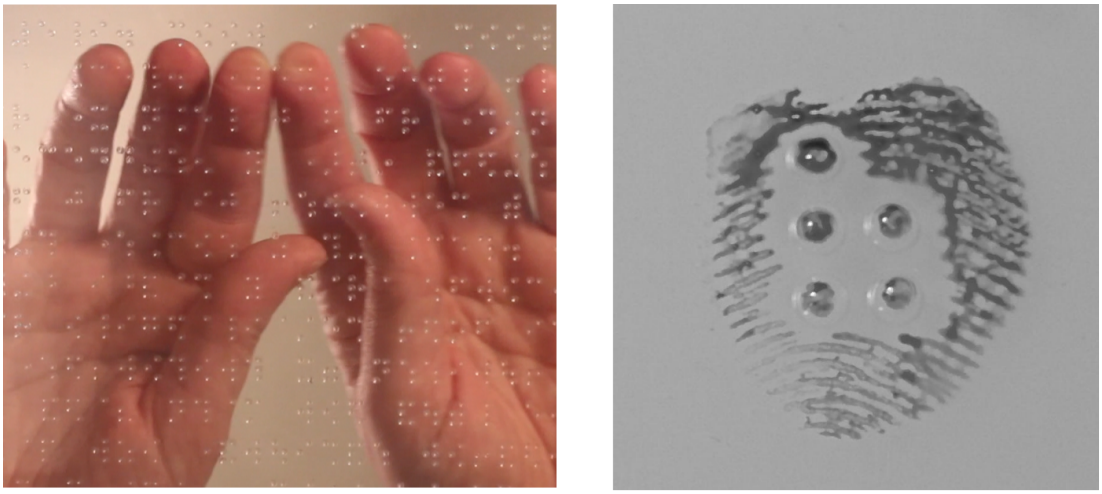

Figure 2.3: Highlighting the contact surface between fingertips and braille characters

the case of sliding indentation (traditional reading by scanning) the contact patch at each pin slides across the fingertip. One pattern slides across, deforming the contact surface into a characteristic shape for the particular braille character being read. As this impression slides off the fingertip to the left, another appears on the right. Because the fingerpulp is soft, the skin could be said to 'flow' across the shape of a braille character to a certain extent.

Tractions acting on the skin are distributed non-uniformly throughout the contact surface. Even within a given contact patch the tractions need not be uniformly distributed. Tractions acting tangential to the contact surface arise from friction effects (sticking or sliding) and tractions acting normal to the contact surface arise from the tendency of the skin to recover its nominal shape while pressed against the braille pins and substrate. Thus the tractions acting on the skin differ markedly depending on whether the finger slides laterally relative to the braille pins (*sliding*) or does not slide (*static*). Lateral motion will produce greater tractions tangent to the reading surface, by virtue of friction forces arising with sliding contact. Static indentations, on the other hand, will produce primarily normal tractions. At an even finer level, the fingerprint ridges may play a significant role in determining the distribution and evolution of tractions. As a case in point, the fingerprint ridges are

known to play a significant role in incipient slip [31].

As the pins move up and down under a finger that remains static relative to the substrate, the fingertip is deformed from a relatively planar surface into a shape that is characteristic for a given braille character and back again. The edges of the contact surface between fingertip and substrate change little. In the case of a sliding indentation, the characteristic surface shape slides across the skin into the contact surface from one side and out the opposite side. I can presume that the stimuli on the mechanoreceptors differ significantly in the 2 cases.

2.4 Methods

Recall the hypothesis, namely that the efficient reading of braille requires the presence of both relative motion between the fingertip and the braille text and proprioceptive input as the hands move across the page (integrated to provide spatial information such as relative position, layout, etc.). The display conditions were therefore chosen to systematically isolate the contributions of these two elements.

2.4.1 Experimental Design

The experiment took the form of a 2-by-2-by-3 within-subject design, with two display types (*static* and *sliding*), two proprioception conditions (*proprioceptive* and *non-proprioceptive*) and three levels of display presentation speed (baseline, fast and slow). The participants were limited to their dominant reading finger for this experiment. As an addendum to the first experiment, two more reading conditions were tested for the TAPE and LINE display configurations. In the first of these supplementary conditions, the participants used both index fingers side-by-side to read, and in the second condition, participants used their dominant reading finger, but read braille in the right-to-left direction.

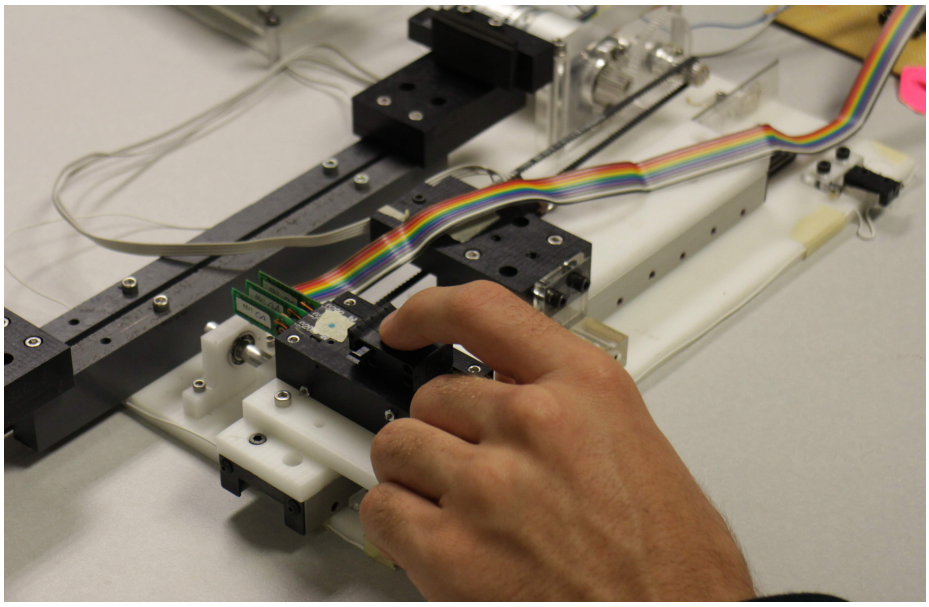

Figure 2.4: Photograph of the apparatus configured for the CLOCK and MOUSE conditions

2.4.2 Participants

Five experienced braille readers between the ages of 19 and 48, with a mean age of 36, were recruited for this study. Participants were recruited from the population of blind individuals working or studying at the University of Michigan and from the local chapter of the National Federation of the Blind. All reported that they could read at a rate of 150 words per minute or greater and read braille on average for at least 1 hour per day. Additionally, all reported that they typically read braille for around two hours in one sitting. Four participants reported being experienced braille readers and one participant reported being an intermediate reader. They also reported that they had no known issues relating to the sensitivity of their fingertips. Due to technical difficulties, only data for four participants is reported in this paper. The participants received no compensation for taking part in the study.

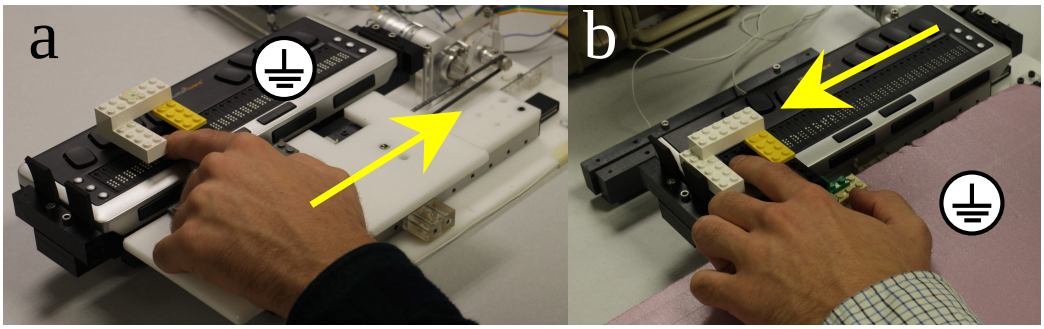

Figure 2.5: Photographs of the apparatus configured for the (a) TAPE and (b) LINE conditions

2.4.3 Apparatus

I built a custom apparatus featuring a motorized platform that could be quickly set up into one of four configurations to test braille reading under the four target conditions. A linear slide (S1-8, Del-tron Precision, Inc., Bethel, CT) constrained the platform to move smoothly along a horizontal line and a DC motor with a gear reduction (IG-32GM 01 Type, Shayang Ye Industrial Co., Ltd., Taoyuan, Taiwan) was used to drive this motion in certain configurations. A linear optical encoder (EM1, 2000 counts/in, US Digital, Vancouver, WA) was used to track the position of the platform. An Arduino microprocessor was used to close the loop while a host computer was used to issue high level commands to the Arduino through a serial interface.

Figures 2.4 and 2.5 show photographs of the apparatus set up in the various configurations. Three items could be mounted alternately to the moving platform: 1) a 32-character refreshable braille display (Brailliant BI 32, Humanware, Québec Canada), 2) a single working braille cell (P16 braille cell, Metec AG, Stuttgart, DE) surrounded by two cells without pins, all extracted from a second refreshable braille display (BrailleLite M20, Freedom Scientific Corp, St. Petersburg, Florida), and 3) a fixture designed to allow the hand to rest on the moving platform while lightly constraining the motion of the finger. The 32-character braille display and the finger-

constraining fixture could also be mounted to ground. The single P16 braille cell was driven at 195 V by the original BrailleLite M20 power supply. The pin deflections for the P16 braille cell and the Brailliant were measured using a digital dial indicator with a 100 mN±15% measuring force (Fowler 54-562-777) to be 0.46±0.03 mm and 0.64±0.05 mm, respectively. Both devices meet the 0.25 mm traditional force measuring reference height for the braille industry [55].

The 32-character braille display was driven by NVDA, an open-source screenreader program for Windows OS. A text file was used to display the desired braille letters for the experiments. The Arduino microprocessor was used to drive the single braille cell via an array of high voltage transistors (ZTX458-ND, Diodes Corp., Plano, TX).

In the CLOCK condition, the single cell was attached to the platform but the platform was not driven. In the MOUSE condition, the single cell was attached to the platform and the platform was driven by the motor. The pins were actuated in a coordinated fashion at fixed intervals equal to standard braille dot spacing (according to the encoder reading) to create the impression of spatially distributed braille characters. In the TAPE condition, the 32 cell braille display was mounted to the moving platform. While the platform was driven to the left, the hand/finger fixture was mounted to ground and the finger was lightly constrained so the braille display moved beneath a stationary finger. In the LINE condition, the 32 cell braille display was mounted to ground while the hand/finger fixture was mounted to the platform. The platform was driven by the motor to the right so the finger was moving across the stationary braille display.

The apparatus also included a unique stereo (2-channel) audio recording system. One channel received audio from a microphone that was attached to the participant's shirt, recording their voice for the experiments to be used in the measurement of letter-detection accuracy and reaction time. The other channel was connected to an analog-output pin of the Arduino microprocessor. For the CLOCK and MOUSE conditions,

Table 2.1: Description of the procedure blocks.

Block	Purpose
1-2	Training
3-6	Reaction time measurement
7-10	Baseline reading speed measurement
11-14	Reading accuracy measurement
15-18	2 fingers and reverse reading

an audio waveform, not audible to the participants, was sent to the recording device every time the single braille cell was actuated. Therefore, the rising edge of the audio waveform corresponded to the presentation of a braille letter. The datasheet for the single Metec P16 braille cell claims a dot rising time of 24 ms. For the TAPE and LINE conditions, the audio waveform was sent at intervals (based on the encoder) equal to the distance between adjacent braille cells. A participant's reading finger was constrained to start in the center of a braille cell, so the rising edge of the waveforms corresponded to the point at which a participant's finger was at the center of a braille cell.

2.4.4 Procedure

Each experimental session took approximately 1 hour and 45 minutes to complete. Participants were presented with a consent form in braille which they read and signed at the start of the session. They were then asked to complete a short pre-test questionnaire (read to them by the experimenter) which established their age, reported reading rate, level of reading experience, handedness, and the average time spent reading braille each day (data from this questionnaire is reported in the 'Participants' section). The experiment consisted of 18 blocks. In each block, participants read letters out loud as they appeared in sequence under a single finger. Each trial of five random letters was initiated with a sequence of two equals signs (all pins

up) and a space (all pins down). The time (or space, depending on the condition) between the cells within each trial was held constant ($\pm \approx 10$ ms) so that the initiating sequence gave an indication of the speed at which the subsequent random letters would appear. The participants were told to read the letters aloud accurately and as quickly as possible.

In the first and second block, participants read five random letters preceded by the initiating sequence from the 32 cell braille display using their dominant index finger and both index fingers placed side by side, respectively. These first two blocks were meant as training blocks, intended to allow participants to become familiar with the way in which letters would be presented. Next, participants completed four blocks (3-6) corresponding to the four experimental conditions. Each condition consisted of five trials of five letters each. The inter-stimulus interval (ISI), defined here as the time interval between the onset of two consecutive stimuli, was set as follows: For the CLOCK case, the ISI was set at a constant value of 500 ms, but for the three other cases, due to the open-loop control of the motor, the ISI was 531 ± 15 ms. The order of the four blocks, which was the same across all participants, was CLOCK, MOUSE, TAPE, and LINE.

The next four blocks (7-10) were used to establish a baseline reading speed for a given participant. The CLOCK condition was used in these four blocks. In block 7 the ISI was set at 750 ms for the first trial and reduced by 10 ms for each subsequent trial until the participant reported at least one incorrect letter in three consecutive trials. In block 8, the ISI was set at 250 ms in the first trial and increased by 10 ms for each subsequent trial until the participant reported all letters correct in three consecutive trials. Blocks 9 and 10 were similar to blocks 7 and 8 and were used to confirm the baseline reading speed. Finally, the ISI values found in blocks 7-10 were averaged to find a baseline ISI particular to a given participant.

The next set of 4 blocks (11-14) corresponded to the experimental conditions

CLOCK, MOUSE, TAPE and LINE (see Table 2.1 for details). The order of these blocks was randomized across participants. Each block contained 15 trials, five for each of three speed conditions, and these 15 trials were also presented in random order. The three speed conditions for each participant were taken as the baseline ISI, 0.8 $\times$ (baseline ISI), and 1.2 $\times$ (baseline ISI) for the baseline, fast, and slow speeds, respectively. For each trial, participants were presented with five letters, and they were asked to speak the name of each letter as quickly as possible.

The last 4 blocks took the form of a 2-by-2 design, with two apparatus conditions, TAPE and LINE, and 2 reading conditions, reading backwards with 1 finger and reading forwards with 2 index fingers side-by-side. The order was randomized across participants. As with previous conditions, the task for participants was to speak aloud each letter as accurately and quickly as possible.

2.4.5 Data Analysis

To determine the relative contributions of (1) the presence of lateral motion (*static* or *sliding*) between the fingertip and the braille text and (2) the presence of proprioceptive cues as the hands move to read braille, I first analyzed the correctness of the participants' responses in blocks 11-14 for the four display configurations (CLOCK, MOUSE, TAPE, and LINE) at each of the three speeds (baseline, fast and slow). The error rate for each participant was calculated for all twelve speed-configuration cases by dividing the number of incorrect responses by the total number of responses for each case. Responses were dropped if there was a technical error (the braille letter was not presented correctly or not presented at all) or if a participant gave no response for any letters within a single trial. If no responses were dropped, there were 25 responses for each speed-configuration case. Errors were recorded during the experiment and then later confirmed from the audio recordings.

I also determined the correctness of the participants' responses for blocks 15-18

in which two different reading conditions (2 fingers forwards and 1 finger backwards) were tested for two configurations (TAPE and LINE).

The stereo audio recording of participants' voice and the waveforms from the Arduino from blocks 3-6 was analyzed to find the reaction times for each letter response for all four reading conditions. Audacity, an open-source audio-editing software, was used to find the time between the leading edge of the audio waveform and the corresponding letter spoken out loud by the participants. Incorrect responses were counted, but no reaction time was calculated when participants failed to report a letter. The mean reaction time for each participant for the four display configurations was found.

The statistical analysis software SPSS (IBM Corp.) was used to analyze the data. To compare the effects of each independent variable on the participants accuracy (in blocks 11-14), a three-way repeated-measures ANOVA (3 speeds $\times$ 2 *static*/*sliding* $\times$ 2 *proprioceptive*/*non-proprioceptive*) was carried out on the mean error rates over the 5 trials in each condition.

The small number of participants due to the specialisation of the population being investigated entails that the power of this analysis was lower than would have been preferred. However, when interpreted in the context of the direction and magnitude of trends in the data, this statistical analysis should allow inference about the likelihood of observed effects being found in replications of this task or related experiments.

2.5 Results

The participants made errors when naming letters more often under the *static* conditions (CLOCK and MOUSE) than under the conditions with *sliding* motion (LINE and TAPE). This trend was intensified with the faster imposed reading speeds. The mean error rates, averaged across four participants, for the 12 cases are shown in Figure 2.6. There was a main effect found for *static* vs *sliding* conditions ($F(1,3) = 10.43$, $p = .048$, $\eta^2 = .67$), indicating that participants produced significantly fewer errors in

conditions with *sliding* motion. A main effect was also found for speed ($F(2,6) = 8.27$, $p = .019$, $\eta^2 = .48$), which indicated that participants error rate increased significantly with increasing display speed. However, the effect of proprioceptive cues on participants error rates was not found to be significant ($F(1,3) = 8.74$, $p = .06$, $\eta^2 = .07$), although it can be noted that the obtained p-value was very close to the predetermined alpha value of 0.05. Additionally, there was a significant interaction found between *sliding* and speed ($F(2,6) = 17.16$, $p = .003$, $\eta^2 = .42$). Visual inspection of the data indicates that this interaction is due to the effects of the *static* vs *sliding* conditions on error-rate being more pronounced at faster display speeds. No other interactions were statistically significant ($p < .05$).

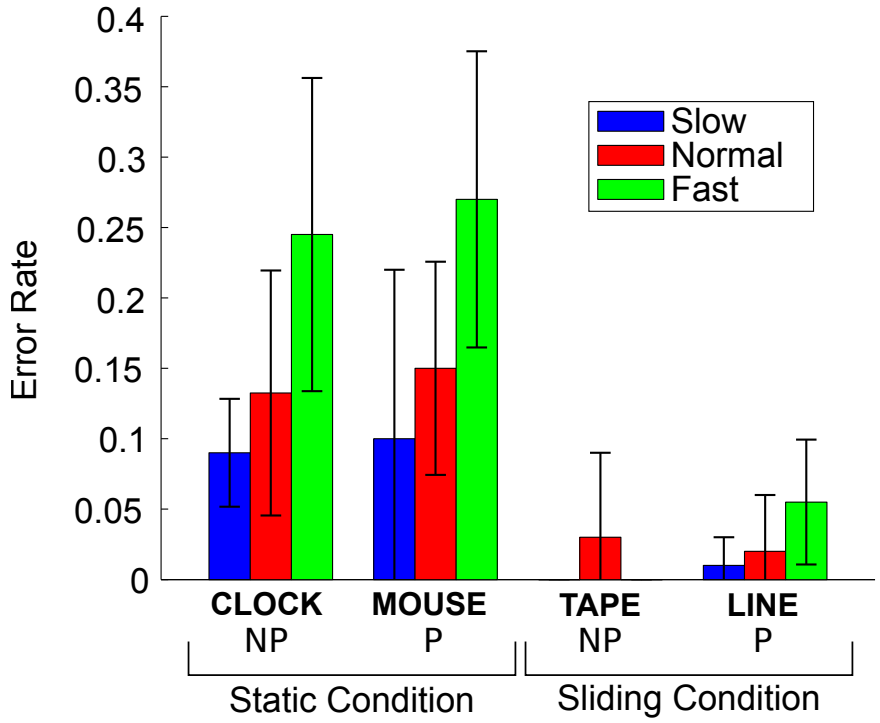

Figure 2.6: Error rates at three different speeds for each reading condition. Error bars represent standard deviations. NP = Non-proprioceptive and P = Proprioceptive.

The reaction time data collected yielded no definitive information. There were issues that arose in the experimental methods that meant it was not appropriate to truly consider it reaction time data. Regarding the supplementary tests, the mean

error rates for all participants were less than 0.06. No discernible trends were seen.

2.6 Discussion

2.6.0.1 Hypothesis I: The Role of Sliding contact

The preferred method of reading for skilled braille readers involves the index fingertips of both hands moving under active control over fixed embossed braille characters or raised pins([43], Chapter 3). But, as stated earlier, the cost of today's braille display technology often motivates a deeper investigation into alternative modes of reading in an attempt to design low-cost products. The aim in this study was to quantify the contributions of sliding contact and proprioception to the recognition of braille letters. the findings indicate that the existence of relative motion between fingertip and braille surface (sliding contact) significantly affects the error rates when reporting letters under timed presentation. For example under the imposed fast reading condition, error rates for the two *static* conditions (CLOCK and MOUSE) were 0.25 ± 0.11 and 0.27 ± 0.11, whereas the error rates for the *sliding* conditions (TAPE and LINE) were 0 and 0.06 ± 0.04. Evidently sliding contact leads to significantly fewer letter identification errors. This suggests that there are more cues available by which to identify letters in the *sliding* conditions TAPE and LINE. It would appear that these findings are consistent with findings of Foulke and Heller reported earlier [19],[25]. However there are some caveats that need to be considered. Firstly, the single-cell display used in the two *static* conditions was drawn from a different refreshable braille product than the 32-character display used in the two *sliding* conditions. The rise times and the bending under load of the braille pins was noticeably different and there was a slight preference for the 32-character display in terms of readability as reported by the participants in post-test interviews. It is further possible that their pin shapes may have been slightly different as, unlike hard copy braille, there is

no official standard for dot shapes, heights and spacing (though most manufacturers follow recommended guidelines such as those cited in [55]). Given that braille readers readily move between hard copy and refreshable braille, this effect, if present, is likely to be small relative to the difference between *static* and *sliding* reading modes. Secondly, participants in Heller's study were shown each letter for up to 15 seconds. In the timed trials, exposure time was much shorter, ranging between 236 ms for fast readers in the fast reading condition to 734 ms for the slowest reader in the slow condition. Exposure to letters in the *sliding* conditions was also slightly longer as, like Foulke, no attempt was made to account for differences in exposure to letters rolling across the fingertip at different speeds; in the *static* conditions, exposure was proportional to speed, but there was a short gap at the end of each exposure (20% of overall interval duration) to ensure that dots shared between consecutive letters would be re-actuated and not merely left in place.

Finally, unlike Heller, the up and down (vertical) sliding motion of the fingertip was not constrained, and I noted that the participants often used up and down sliding motion, especially in the MOUSE condition. A interesting area of future work is the motion analysis of the high-speed video recordings to determine whether readers used different finger movement strategies in the *static* and *sliding* conditions, particularly since the participants were skilled braille readers and Heller's were not [25]. One interesting hypothesis concerning sliding contact conditions is that of tactile flow. It is possible that not only the presence of sliding but also the direction of sliding provides cues to braille readers that are similar to directional cues available from invariants in visual stimulation on the retina [21]. To test this hypothesis, a supplementary sliding condition in which the display moved across the fingertip from left-to-right was included. Thus letters were encountered one-by-one, as before, but the direction of sliding was opposite. When compared to the forward case, however, no detectable differences in error rate were observed.

2.6.0.2 Hypothesis II: The Role of Proprioception

the second hypothesis, that proprioception would contribute to error rates, was not supported. the expectation was that the presence of proprioception, even passive proprioception, would improve reading, compared to the cases without proprioception. This was not borne out by the data. The effect of proprioception on error rate did not reach significance, and although the p-value of this analysis was close to .05, which would suggest that a larger sample size might produce a significant effect, the effect size was substantially smaller than that found for speed and the sliding/static comparison. Moreover, the trend obtained was for proprioception to increase error rates. Hence, I can conclude that, in this study, displays that modulated proprioception did not lead to improved performance. As Gibson noted [20], active touch, where the observer is in complete control of the pacing and direction of their exploratory movements, yields much better performance in shape recognition and length estimation tasks. In a pilot study, I attempted to introduce some element of control of character presentation by providing participants with a button that they could press with their non-dominant hand to cause letters to appear on the braille display in all conditions. Even this self-pacing, however, was not sufficient to promote the tight sense of coupling between movement and stimulus pick-up equivalent to free reading of text. In fact participants found the need to trigger letters distracting and quickly outpaced the display in the proprioception conditions for both *static* and *sliding* cases. The implications of the findings for the design of refreshable braille displays are that displays that update-in-place, like the *static* conditions, are likely to be less successful than displays that allow for sliding contact between the fingertip and the reading surface. This finding is borne out by the fact that attempts to commercialise such displays have historically met with little success in the marketplace, even given their extreme cost advantage.

Table 2.2: Participants' rankings of reading method from easiest (1) to hardest (4).

Participant #	1^{st} Choice	2^{nd} Choice	3^{rd} Choice	4^{th} Choice
1	CLOCK	LINE	MOUSE	TAPE
2	LINE	TAPE	MOUSE	CLOCK
3	LINE	TAPE	CLOCK	MOUSE
4	LINE	TAPE	CLOCK	MOUSE

Though not specifically addressed in this current study, the findings might also have implications for the design of tactile graphics using an array of pins. While the relationship between braille letter identification errors and recognition of shapes, orientation, or contour geometry might be complex, some conjectures could nevertheless be made. Cues from sliding contact are evidently very important for recognizing the shapes of braille characters and it is possible that such cues might be important for contour following as well. Since I found the MOUSE condition was associated with higher error rates, I might presume that discriminating fine detail in a tactile graphic or tactile map might be more difficult when using a MOUSE display than when using a full grid pin array. Furthermore, navigating a diagram with a tactile mouse introduces other orienting issues such as parallax errors arising from the lack of visual feedback to coordinate the movement of the mouse with that of the cursor on a screen. While such effects have not been documented for tactile mice, there is evidence that blind optacon users have difficulty tracking lines on a page with the hand-held reading camera [27]. Given that the MOUSE condition was constrained to a straight line, there was no possibility for straying from the text and yet participants still performed poorly in this condition and liked it least (See Table 2.2).

However, given that the proprioception conditions (MOUSE and TAPE) were both passive, the results should not be taken as evidence that there is no role for proprioception in braille reading. Heller's findings with blindfolded participants already point to improved performance when active touch is available. Further, if the stimuli were not letters but were words, where there is a spatially extended semantic unit,

it is likely that any results for either active or passive proprioception conditions with single letters would not hold.

A further factor to consider for the proprioception conditions (MOUSE and TAPE) is that participants were only reading with one finger. This is a somewhat unrealistic scenario for skilled readers who typically employ a so-called 'butterfly' technique. In this technique, the hands continually converge and diverge as they advance down a page of text, with the right hand reading the end of a line while the left hand tracks back to locate the start of the next line. For at least half of each line, the fingertips cross over letters in sequence, effectively providing two chances to read each symbol. It is still not clear how focal awareness shifts between each reading finger [43]. Though electronic braille displays usually have only one line, most readers carry this efficient technique over from hard copy reading. In order to establish whether two fingers would improve performance over a single finger in the *sliding* condition, I carried out a supplementary test comparing error rates for the one-finger tape condition with a condition where the two index fingers were placed side-by-side and moved across the 32 cell braille display. Error rates for both conditions were very low, suggesting that there was no benefit to adding a second finger to the passive proprioceptive condition. Given that participants could not employ the butterfly technique, however, it is likely that this condition is not representative of free two- finger reading performance.

Finally, it must be noted with regard to the p value of 0.06 associated with the effect of proprioception in the study that although more participants and stronger power might lead to a reduction in p-value, it is just as likely that the analysis could go the other direction. Further testing would be necessary to confirm the lack of effect found in this data set.

It is interesting to note the detrimental effect that speed of display had on performance accuracy, and particularly that the interaction effect showed that this detriment was most pronounced in the static display conditions. This result would indicate

that rate limits imposed on letter comprehension are reduced for sliding conditions where lateral contact motion is present, which in turn has implications for developing displays that can lead to faster reading rates for braille users.

2.6.0.3 Reaction Time

One further way to compare performance across the four display conditions might be to compare the time that participants took to recognise and name letters in each case. I therefore developed a method of capturing the time of a stimulus onset (alongside the verbal response of the participant) in a 2-channel audio recording. The hope was that the calculate reaction times could be calculated from this data. However, it soon became clear that presenting stimuli as sets of five timed letters was causing participants to process the incoming stimulus while they were trying to verbalise the preceeding letter, even for slow reading speeds. When the ISI was relatively large, participants would adopt a cadence in their verbal responses that was dictated by the pace of the stimulus presentation and was not indicative of reading the letters as quickly as possible. I was therefore unable to extract any conclusive results from this data. A more effective test would involve giving participants a single letter at random time intervals.

2.7 Conclusions

The hypotheses were that the presence of both sliding motion and proprioceptive cues would help in reading braille. The results of these experiments indicate that continuous slip is indeed important in enhancing accurate comprehension of braille letters, but that (passive) proprioceptive information does not confer a similar advantage for reading accuracy. This suggests that single-cell displays that do not incorporate sliding contact are likely to be less effective for braille reading than displays which do incorporate sliding motion.

CHAPTER III

Modeling and Design of Pressure-Controlled Valves for a Refreshable Tactile Display

3.1 Introduction

Current commercial refreshable braille displays (RBDs) are expensive and bulky, mainly due to the complex piezoelectric bimorph technology used to create the raised dots. This effectively limits the displays to one or two lines of braille for portable devices, making reading difficult and displaying tactile graphics impossible. Simple experiments reveal that haptic technologies that are unable to modulate the distribution of forces within the finger contact patch are not suitable for braille reading [79]. Therefore, technologies that rely on electrostatics and electrovibration, which work by modulating frictional forces uniformly across the contact patch, are not able to render standard braille in their present form [72, 13]. Further, studies have demonstrated the importance of sliding contact between the fingertip and braille reading surface [60]. As such, displays that reduce size and cost by restricting the display to a single braille cell (think single braille cell on a mouse) are likely to be less effective for braille reading.

There are many actuator technologies that have been adapted for refreshable braille and tactile display applications. Belt and tape drives were introduced as a

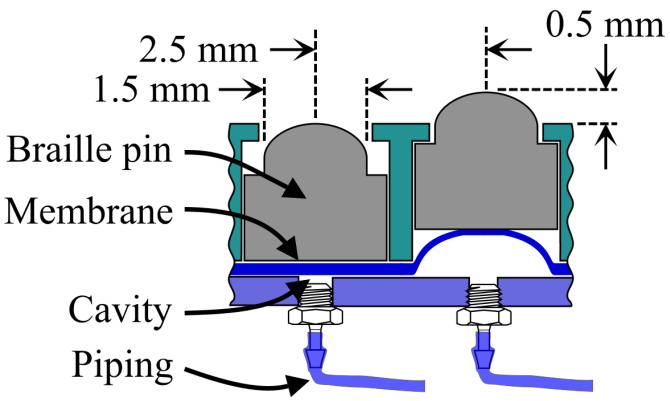

(a)

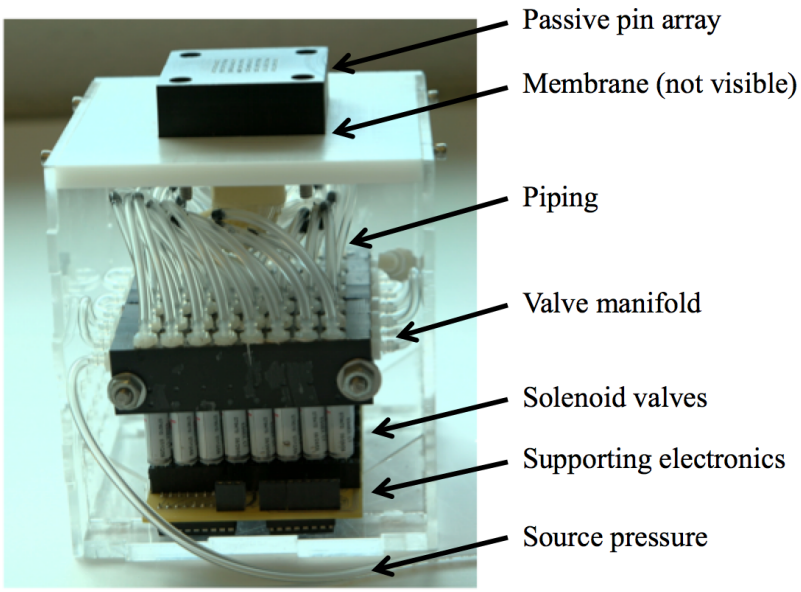

(b)

Figure 3.1: (a) A side view of a pneumatic actuator design. Small channels or pipes route pressurized fluid (air or liquid) to small cavities. A thin elastic membrane above the cavities deflects upwards forming a bubble when pressurized. The bubble can be touched directly or as pictured here, move a sliding pin held within a passive array, thereby separating the bubbles from contact with fingers. (b) A realization of the pneumatic actuators interfaced with a passive array. A 7x8 array of braille-sized pins is pictured.

means of maintaining sliding contact while reducing the number of actuators needed [55]. Many other technologies are still being pursued today including thermal actuators, shape-memory alloys (SMA) or thermal wax expansion, electro-active polymers

(EAP) [4], and solenoids [55]. For a more in depth review of technologies being implemented for refreshable braille and tactile displays, see [72, 6]. However, piezo-electric actuators remain the only technology found in commercially available RBDs. The cost for a single piezo-powered braille cell (single character) is about 100 US$ to the end user, setting the price of even single line RBD well over 1000 US$ [54]. Therefore, the search is still on for a low-cost full-page refreshable braille display.

3.1.1 Pneumatic Actuators for Refreshable Braille

Pneumatic actuators show promise for refreshable braille and tactile display applications. The advantage of using pneumatics is that the power source is divorced from the actuator. Power, in the form of pressurized air, is routed via small pipes and readily converted into the motion of a sliding pin using an elastic membrane. Separating the power source and means of modulating the power (e.g. valves) from the actuation point allows for many pins to be tightly packed together to form a large-area dense array shape display. The use of pneumatic actuators for rendering refreshable braille and tactile graphics has been proposed previously [80, 78, 6, 52]. To motivate further research on pneumatic actuators for refreshable braille, I built a pneumatically-driven tactile display based on the design pictured in Fig. 3.1a. The realization of the display design, shown in Fig 3.1b, uses the deflection of a thin-film elastic membrane above pressurized cavities to drive a 7 8 array of mechanical pins. The display was shown to meet the force, spacing, and deflection specifications for refreshable braille [58, 57]. The display supports two lines of braille text, each consisting of three six-dot letters. A tactile graphic with 56 pixels can also be rendered. A braille pin sits in the top plate and slides freely up and down based on the deflection of the membrane under pressure. The pin returns to an inactive state under the action of gravity if the membrane is depressurized. The membrane acts as the actuator element, converting pressure into mechanical force and displacement, and

provides a seal for the system. The pressure to each pneumatic actuator is controlled by a solenoid valve. Each valve is fixed to a common manifold that is maintained at a constant pressure from the source and connected to a single cavity by elastic tubing. The valves are controlled using a microprocessor coupled with supporting electronic circuitry. As pictured in Fig. 3.1b, the size of the supporting control circuitry (piping and electronics) for an actuator array is large relative to the array size. Each tactile dot requires a dedicated external control valve and pipe, which severely limits the portability and scalability of the design.

The difficultly of controlling a large array of pneumatic features related to the required valves and pipes for each element has limited their successful implementation in refreshable braille. I propose that the complexity associated with controlling pneumatic devices can be reduced by adding integrated fluidic logic networks. Fig. 3.2 shows a conceptual design of a fluidic logic system integrated with pneumatic actuators to drive braille pins. In such a realization, each pin is addressed by a pneumatic actuator and a basic fluidic latching memory unit. The fluidic memory units function using pressure-encoded binary signals (high and low pressure) that enable individual actuators to be addressed and controlled without dedicating an external pressure control feature to each actuator. For example, a latching shift register would allow a row of actuators to be addressed using a small number of control channels. Similar to how the very-large-scale integration (VLSI) movement enabled mass scaling-down of electronic logic circuits to a single chip, fluidic logic networks enable the large-scale integration of fluidic elements [66]. By significantly reducing the need for external control features, the pneumatic RBD can be scaled to meet the cost and display size needs for braille users. Specifically, the tactile display could work much like active-matrix LCDs introduced in the 1970s. Basic electric circuits, repeated for each pixel, are built directly into LCD displays using thin-film transistors (TFTs) [7]. The circuits are X-Y addressable and crucially, are latching, allowing them to store the

electrical state of each pixel as the display is updated. Applying this to pressure-based tactile displays would reduce the required number of external control valves from many thousands (one for each tactile feature) down to just a few.

Fluidic logic systems were first developed in 1959 and researched extensively in the early 1960s [75]. More recently, microfluidic logic systems have been under development for large scale lab-on-a-chip analytic operations that enable parallelization of biological research processes. Some approaches have focused on using droplets or bubbles as Boolean states, but these are not suitable for producing haptic features to be felt by a finger [12]. Many logic systems have also been created based on binary pressure levels. Some designs fail because the pressure output of one element is not sufficient to actuate subsequent elements [50] or fails because certain elements lose their state (on or off) after a period of time [22]. In others, signal strength decays from element to element requiring amplification [30]. Lastly, in some designs the input and output signal types are different, preventing the output of one element from controlling the input of another [71].

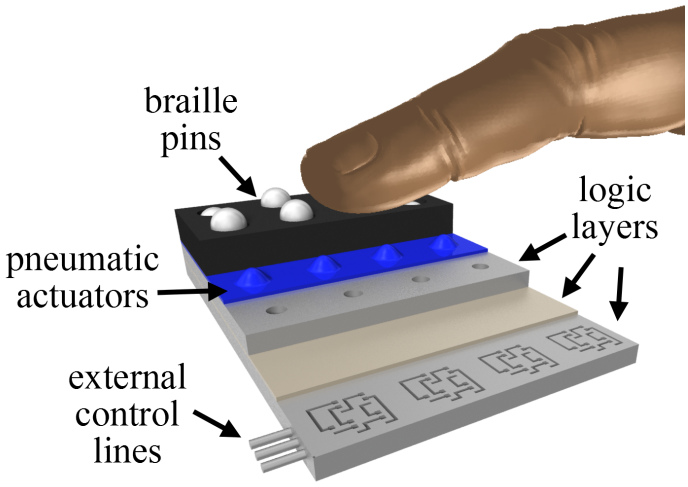

Figure 3.2: An integrated fluidic logic and actuator system for surface haptics.

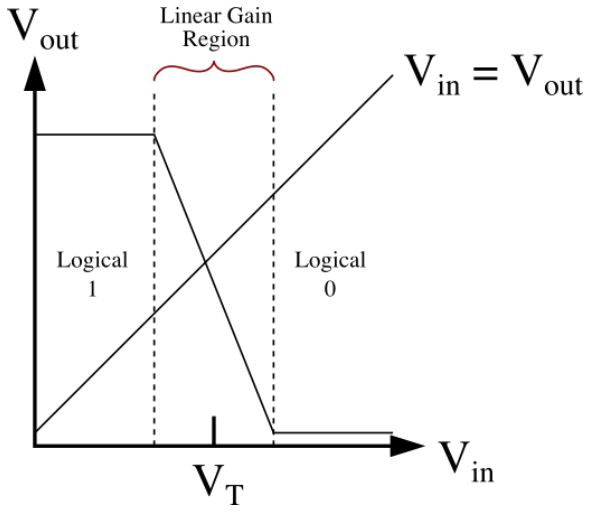

Figure 3.3: Voltage Transfer Curve for Electronic Inverter.

3.1.2 Digital Abstraction in Microfluidics

Key to the design of complex fluidic logic is the ability to cascade any number of embedded control features without loss of signal or function. In an electronic analogy, this is achieved by implementing transistors that have (1) non-linear gain and (2) a voltage threshold V_T between the high and low system voltages. An example of a resistor-transitor logic (RTL) inverter voltage transfer curve, which is a way to visualize transfer characteristics for a logic feature, is shown in Fig. 3.3. The nonlinearity of transistors divides the input voltage range into two regions with near-zero gain separated by an input voltage region with negative gain (linear region in Fig.3.3). The presence of the two large regions with no gain provides two distinct logic levels, enabling digital abstraction. Transistors with nonlinear gain and voltage thresholds between the high and low system voltages enable circuits with only marginally valid inputs to produce outputs that are valid [74, p.12]. Ideally, the linear gain region around the voltage threshold is infinitesimally small and must be between the high and low system voltages. In that way, circuits always produce valid output signals and thus are infinitely cascadable.

Many groups have presented microfluidic logic designs that achieve cascadabil-

ity by implementing both vacuum- and pressure-based (above atmospheric pressure) fluidic valves with non-linear gain and thresholds between the high and low system pressures.

The construction of vacuum-based valves is well-documented [51, 15, 22, 23, 30]. For vacuum-based valves, when vacuum pressure is applied as an input to the gate, the valve opens, allowing fluid flow across the valve, whereas an input of atmospheric pressure closes the valve, preventing fluid flow. A key benefit of vacuum-based designs is that layers of devices are reversibly bonded, simplifying the fabrication process [51]. That is, all pressures are below atmospheric pressure within the device, so it can be held together with a weak bond. Importantly, vacuum-based valves are formed at the contact of two layers of the device. In order for the valve to function properly, the contact in that area is broken upon an applied vacuum pressure. Therefore, avoiding bonding in the valve area is necessary for the valve to function properly. Methods exist for selectively bond layers without bonding the valve area, but they require more complex fabrication techniques [46]. Vacuum-based valve designs have been shown to achieve non-linear gain and thresholds between the high and low system pressures. More recently, pressure-based valves have been proposed which require more complex fabrication techniques. With the tendency of pressure (above atmosphere) to cause device layers to split apart, more permanent adhesion methods must be used. Therefore, different fabrication techniques are needed to achieve a working valve structure. As described earlier, a fluidic valve is formed where two device layers make contact. If using the same design as vacuum-based valves, the stronger adhesion methods result in the membrane permanently bonding to the valve seat (without selective bonding techniques). Therefore, different design techniques are needed. In one such case, Weaver, et al. present a design that achieves gain using embedded SU-8 discs [76]. However, fabrication requires more complex processing techniques involving vias and SU-8 patterning on a PDMS substrate. Additionally,

while the valves achieve non-linear gain behavior, the logical HI output signal is half the source pressure and only marginally valid, so the signals degrade when circuits are cascaded [76]. Another pressure-based valve design is presented by Devaraju et al. that achieves nonlinear gain in a working cascadable circuit [14]. Fabrication requires post-processing of the chips by injecting a UV flash-curable material and curing under pressure. The flow layer within the area of the control channel is deformed into contact after layers are cured together. The resulting valve design is similar to vacuum-based designs, but with an additional design parameter corresponding to deforming the valve seat further into the control layer.

While many elastomer-based valves have been presented in microfluidic logic literature, some of which have been shown to achieve important attributes for digital abstraction, models are not available to relate fluidic valve design aprameters to performance criteria such as cascadability in logic circuits. Rhee et al. discuss valve performance in logic circuits as it relates to a parameter called area fraction, but only offer an experimental assessment of the influence of area fraction on valve behavior [51]. Additionally, Duncan et al. [15] and Mohan et al. [44] study design considerations for valves, but these groups do not offer any parametrized models in support of design decisions. Additionally, several papers explore the performance of stand-alone fluidic valves, but not as they are applied in fluidic circuits [62, 18, 33].

In this work, a first-principles mechanistic model is proposed that predicts nonlinear gain behavior and pressure thresholds based on varying fluidic valve design parameters common to vacuum- and pressure-based microfluidic valves in the literature. The model captures the relative contribution of fluidic valve design parameters toward achieving digital abstraction in cascadable fluidic logic circuits.

Section 3.2 describes a microfluidic valve design common in the literature and introduces key attributes for supporting digital logic functions. Section 3.3 introduces a mechanistic model of the fluidic valve implemented in a fluidic inverter circuit. Sec-

tion 3.4 presents analysis of model design parameters and an experimental validation. Section 3.5 describes key findings from the model analysis and presents experimental results that contribute to validation of the model. Section 3.6 summarizes the conclusions and contributions of the work.

3.2 The Microfluidic Fluidic Valve

3.2.1 Building Blocks

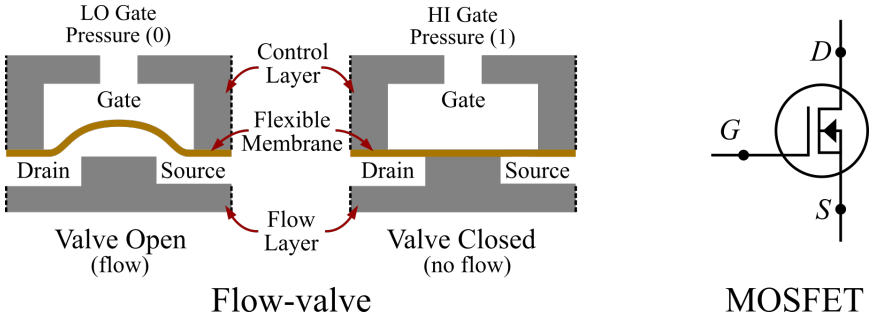

Figure 3.4: Cross-sectional views of a pressure-based fluidic valve in the open and closed states.

Fig. 3.4 shows a cross-sectional view of common design for a fluidic valve in closed and open configurations. This design is implemented in various forms in both vacuum- and pressure-based designs [51, 15, 22, 23, 30, 14]. The valve is constructed by placing a flexible membrane between two fluid channel layers, referred to here as the control layer (top) and the flow layer (bottom). An impediment in the flow channel, referred to here as the valve seat, makes contact with the flexible membrane in the area of the control channel and thereby separates the flow layer channel into two sections. The resulting three-terminal device works analogous to a metal-oxide-semiconductor field effect transistor (MOSFET), shown in Fig. 3.4 on the right, in which voltage and current are analogous to pressure and fluid flow. With a positive drain-source voltage, a zero gate voltage enables the largest current flow while a sufficient positive voltage to the gate stops current flow. Previous work drawing comparisons between

microfluidic fluidic valves and MOSFETs in this manner can be found in [63, 64, 30]. Preserving the comparison to the MOSFET, the terminals of the fluidic valve are referred to as the gate G, drain D, and source S, as pictured in Fig. 3.4. The gate pressure P_G controls the fluid flow between the drain and source. Since the control layer is separated from the flow layer by the membrane, the valve gate does not draw or source any fluid flow. Under an applied positive differential pressure in the flow channel between drain and source, when there is no positive gate pressure, the membrane deflects upward connecting the drain and source, and the valve allows fluid flow. When sufficient positive pressure is applied at the gate, the membrane makes contact with the valve seat and fluid flow across the valve is stopped. With no gate pressure, any applied drain-source pressure results in flow, so the valve can be referred to as a normally-open valve or in its electronic analogy, a normally-closed switch or normally-on transistor.

While the naming convention for the binary states of vacuum- and pressure-based valves are opposite in the literature, the valve function in each case is the same. For a system-wide high and low pressure, a relatively higher pressure closes a valve and a lower pressure opens the valve. For pressure-based designs, a pressure applied at the gate that results in a closed valve, preventing fluid flow between drain and source, is considered a logical HI (1). Any gate pressure that results in an open valve, allowing fluid flow between drain and source, is considered a logical LO (0). Some vacuum-based valves in the literature, e.g. [51], follow the opposite convention, with the lower pressure (vacuum) that opens the valve being considered a logical HI (1) and the higher pressure (atmosphere) considered a logical LO.

3.2.2 Defining Binary Valve States

Two different states are possible for fluidic valves: open and closed. When the valve is in an open state, there exists a minimum gate pressure P_G that will close the

valve, which is referred to in this work as the *valve closing pressure* P_{cl}. When the gate pressure P_G increases to reach P_{cl}, the valve closes, stopping fluid flow across the valve. When the valve is in a closed state, there is then a minimum gate pressure P_G that will keep the valve closed, which is referred to in this work as the *valve opening pressure* P_{op}. When the gate pressure P_G decreases and drops below P_{op}, the valve opens and fluid flows from drain to source. Unlike MOSFETs, fluidic valves have been shown to have two different thresholds for the opening and closing conditions [51, 14, 15]. The phenomena giving rise to distinct opening and closing thresholds will be further discussed below.

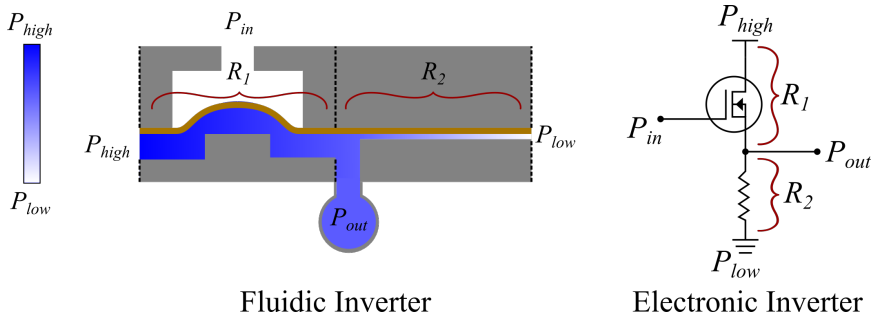

Figure 3.5: Cross-sectional views of a pressure-based fluidic inverter with the fluidic valve in an open state. The input is LO and the output pressure is HI due to the pressure drop across the pull-down resistance R_2

The importance of nonlinear gain and valid pressure thresholds in fluidic valves for achieving digital states in cascaded circuits is best described using a simple logic circuit example. In analogy to resistor-transistor logic, an inverter, i.e. NOT gate, is realized by placing the fluidic valve in series with a pull-down resistive line (or constriction). A high pressure source is attached to the valve drain, and a low pressure source is attached to the end of the resistive line. Fig. 3.5 shows the fluidic valve described in Sec. 3.2.1 implemented in an inverter circuit. The inverter produces a logical output state opposite to its input state. When the valve is closed, there is no fluid flow, so the output pressure of a NOT gate is equal to the low pressure P_{low}, referred to as $P_{out,LO}$. Therefore, in a cascaded circuit, in which the output of the

first inverter is the input of the second, the subsequent valve gate should open under conditions where the input is no smaller than $P_{out,LO} = P_{low}$, giving the following design requirement:

$$P_{op} \geq P_{low}. \tag{3.1}$$

When the valve is open, the circuit acts analogous to a voltage divider, so the HI output pressure $P_{out,HI}$ can be estimated as:

$$P_{out,HI} = (P_{high} - P_{low}) \frac{R_2}{R_1 + R_2} + P_{low}, \tag{3.2}$$

where R_1 and R_2 are the fluid resistances of the valve and pull-down resistive line, respectively. Therefore, in a cascaded logic circuit in which the output of one logic gate is the input to a second gate, the input to the second NOT gate will be less than P_{high}. For the second logic gate to function properly, the output pressure of the first circuit when applied at the valve gate of the second must be strong enough to close the valve, giving the following design requirement:

$$P_{cl} \leq P_{out,HI}. \tag{3.3}$$

In addition to the requirements of Eq. 3.1 & 3.3, the valves must have nonlinear gain. The range of input pressures between P_{high} and P_{low} should be divided into two valid logic regions with near-zero gain, separated by a middle region of high negative gain. Any signal loss from one element to the next should still produce valid input signals and not propagate [74, p. 12].

The relationships described above represent two essential features for fluidic valves that enable cascadable logic circuits: (1) the opening and closing pressures must lie between the lowest logic circuit output pressure and system-wide low pressure and (2) the valve must exhibit nonlinear behavior, providing two distinct logical levels.

3.3 Flow-Valve Model Description

A parametrized model is now introduced that describes the gain behavior, pressure thresholds, and output pressures of a fluidic valve implemented in a simple logic circuit. The model incorporates parameters related to common design features of microvalves implemented in logic circuits in the literature.

3.3.1 Assumptions

The following assumptions are made in the construction of the model that follows: 1) The fluid flow resistance of the valve as the gate pressure increases is taken to be constant until the valve closes. 2) The width and height of fluid channels, which contribute to fluid resistance, are neglected. 3) Dynamic effects are neglected. That is, the model describes the mechanistic behavior of the membrane under fully-developed static pressures.

3.3.2 Model of Fluidic Valve in an Inverter Circuit

The operation of a membrane-based fluidic valve can be described by a model that drasitcally simplifies the mechanics of the membrane. The tendency of the membrane to seal against a valve seat is predicted by a spring. Valve seat geometry is critical to the design of a valve that achieves cascadable function. The parametrized valve model is pictured in Fig. 3.6, with the valve in series with a pull-down resistive line between high and low pressures. The relative resistance between the valve R_1 (owing to the constriction between the valve seat and the membrane) and pull-down resistance R_2 is parametrized as $R = R_2/R_1$. The flexible membrane is modeled as a rigid plate and spring that operates to open and close the connection between the drain and source channels. The plate seals the gate chamber from the drain and source channels and slides along frictionless cavity walls under the action of a nonlinear spring force F_{sp}, the action of gate pressure, and the action of pressure in the flow channel. The valve

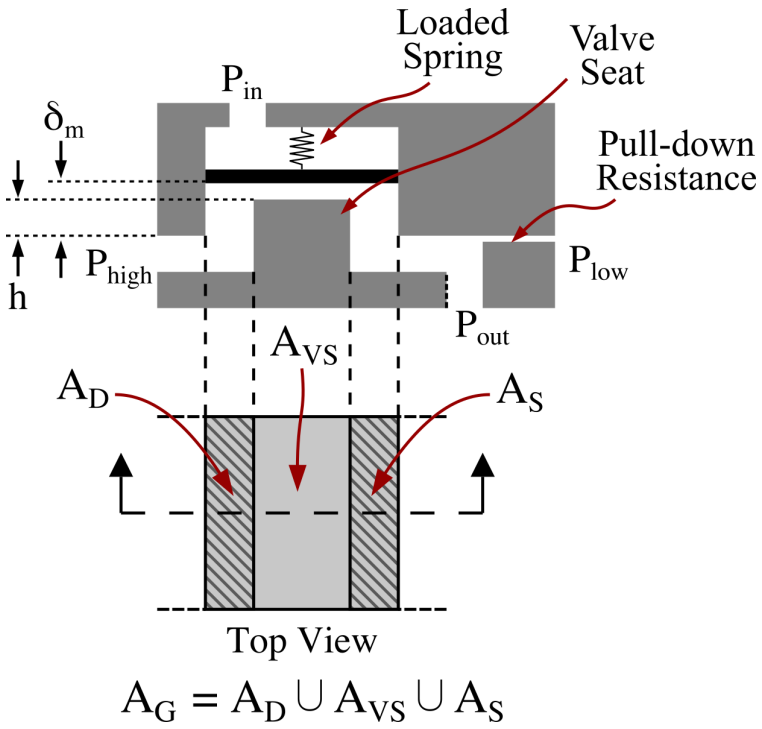

Figure 3.6: A rigid plate model of the fluidic valve configured in a NOT gate. The valve membrane is modeled as a rigid plate attached to a spring. The valve seat with area A_{VS} is protrudes by an amount h into the top control layer.

seat (the ridge that separates the drain and source) height h is a design parameter that corresponds to a protrusion of the valve seat into the control layer. When the valve seat height h is 0, the spring is at its free length, corresponding to a relaxed membrane. The basis for the addition of this design parameter relates to pressure-based valve designs described by Devaraju et al. [14] and Weaver et al. [76] that have positive and negative equivalent valve seat heights, respectively. The force on the plate due to the spring F_{sp} is modeled from the equation for the deflection of a thin square membrane (deflection greater than thickness) under pressure [61]. Assuming no residual stress, the center deflection δ_m of a thin square membrane is related to the pressure drop ΔP across it by: [61]:

$$\Delta P = C\delta_m^3. \tag{3.4}$$

where C is referred to as the membrane stiffness, with units Pa/m^3, and is a lumped parameter related to the Young's Modulus and Poisson's ratio of the material, and the geometry of the membrane (e.g. thickness, side length). The restoring spring force due to a valve seat height h is modeled as being related to the amount of pressure applied over valve area A_G required to deflect the center of the membrane by an amount h from its free length. The restoring force of the spring F_{sp} in the closed condition due to a valve seat height ΔP is obtained:

$$F_{sp} = Ch^3 A_G, \tag{3.5}$$

where A_G is the area of the membrane exposed to the gate pressure.

Relevant areas and pressures are defined in Fig. 3.6. When the valve is closed, there is no fluid flow and the flow pressure P_{high} acts over area A_D. When the valve is open, there is a pressure drop across the valve. The pressure acting on the bottom part of the rigid plate over area A_G is considered to be the average of P_{high} and P_{out} based on Eq. 3.2 due to the pressure gradient. We define a design ratio that represents the geometric relationship of the valve area to be a dimensionless parameter called the *area fraction*,

$$f = \frac{A_D}{A_G} = \frac{A_S}{A_G} = \frac{A_G - A_{VS}}{2A_G}, \tag{3.6}$$

where A_{VS} is the area of the valve seat, and the drain area A_D and source area A_S are considered equal so the valve is symmetric. A similar design ratio for fluidic valves is described by Rhee et al. [51]. Note that the area fraction f is always less than 0.5, enforcing a condition that there is a valve seat present in the flow channel.

The opening and closing pressures of the valve are to be determined based on the model described above. In the closed state, the high pressure at the valve drain P_{high} acts over area A_D and the input pressure P_{in} acts at the valve gate over a larger area A_G. By first applying a force balance on the rigid plate in the closed configuration,

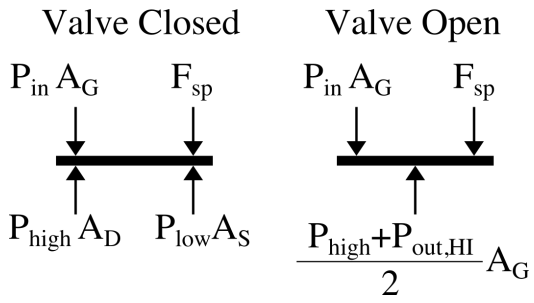

Figure 3.7: A force balance of the pressures and spring force acting on the rigid plate shown in Fig.3.6.

shown in Fig. 3.7, and then applying the area fraction relationship from Eq. 3.6 and the spring force relationship from Eq. 3.5, the following relationship is obtained:

$$P_{op} = f \times (P_{high} + P_{low}) - Ch^3. \tag{3.7}$$

A spring with no pre-load h is at its free length ($\delta_m = 0$) and provides no force when in the closed position, so the opening pressure will be equal to $f \times (P_{high} + P_{low})$. With added pre-load corresponding to an added valve seat height h, the valve is closed when the spring deflection δ_m is equal to the height h. The added pre-load acts to lower the input pressure P_{in} required to keep the valve closed.

In the open state, the fluid resistance of the valve R_1 results in a pressure drop across the valve. Based on this pressure drop, the pressure acting over the gate area A_G on the flow side of the membrane is taken to be the average of P_{high} and $P_{out,HI}$ (based on Eq. 3.2). From the force balance on the rigid plate in the open state, shown in Fig. 3.7, the input pressure that causes the valve to close, i.e. the valve closing pressure P_{cl}, is obtained as:

$$P_{cl} = \frac{P_{high} + P_{out,HI}}{2} - Ch^3. \tag{3.8}$$

Applying the relative resistance $R = R_2/R_1$ and setting the low system pressure P_{low}

to be 0, the HI output pressure from Eq. 3.2 simplifies to:

$$P_{out,HI} = P_{high}\frac{R}{R+1}. \tag{3.9}$$

3.4 Results

3.4.1 Model-based Parameter Sensitivity Analysis

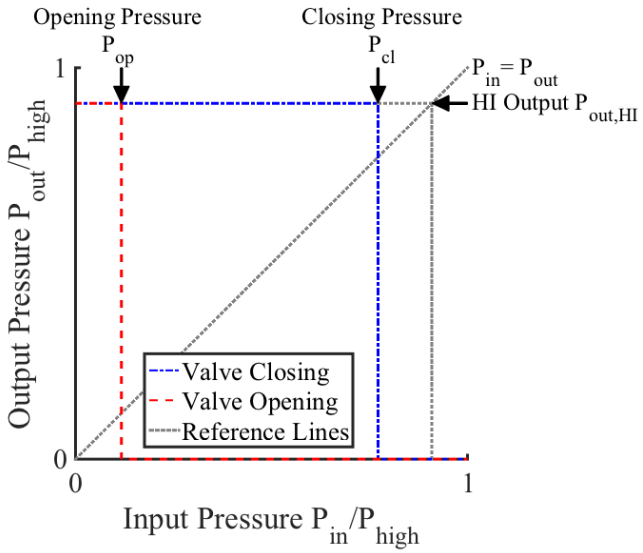

Figure 3.8: A pressure transfer curve for an inverter with chosen design parameters. The blue trace represents an increasing input pressure P_{in} to close the valve and the red trace represents a decreasing input pressure P_{in} to open the valve. The opening and closing pressures are found as the input pressures that open and close the valve, respectively. The HI output pressure $P_{out,HI}$, while characteristic of the output pressure (vertical axis), is plotted for the input pressure to show its relation to the closing pressure.

The mechanistic model developed above was used as a basis for an analysis of sensitivity of critical performance criteria for cascadability to certain design parameters. The pressure transfer curve, a plot of output pressure versus input pressure, is a useful means of describing key functions of the fluidic valve as a logic circuit element. Fig. 3.8 shows a characteristic pressure transfer curve for an inverter circuit based on the model, annotated with key values including system pressures P_{high} and

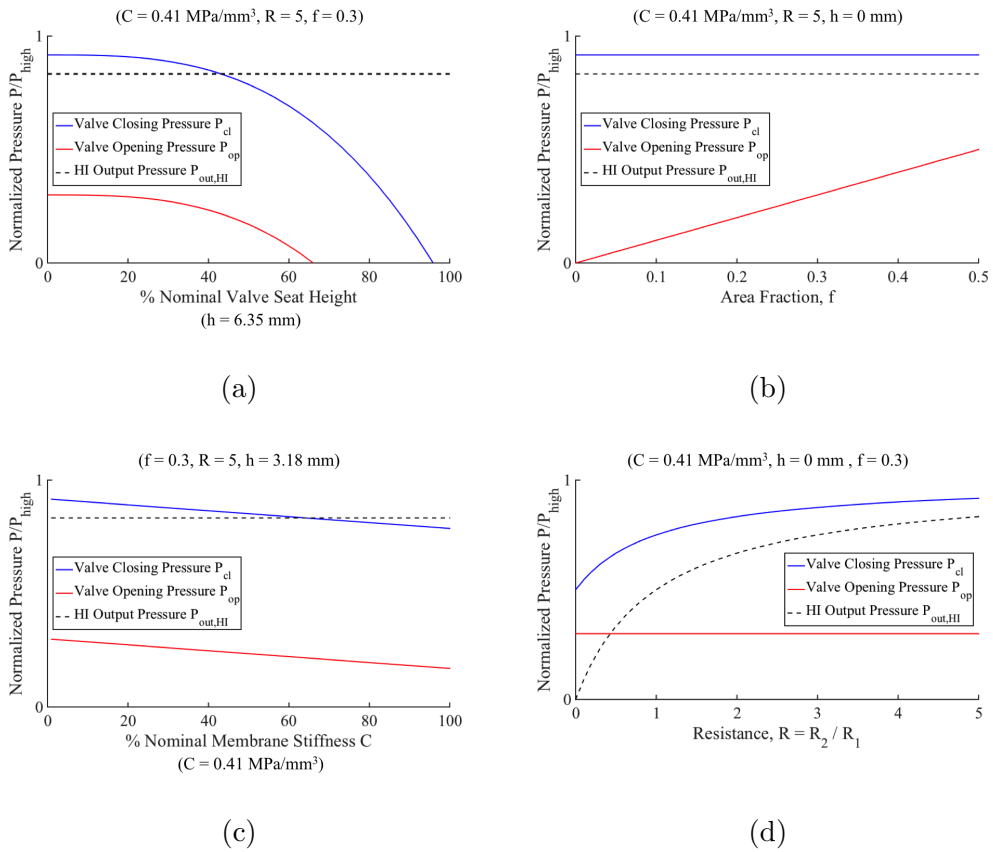

Figure 3.9: Sensitivity of normalized opening, closing, and HI output pressures with respect to (a) pre-load h, (b) area fraction f, (c) membrane stiffness C, and (d) relative resistance $R = R_2/R_1$.

P_{low}, opening and closing pressures, and the logical HI output pressure from Eq. 3.2. Fig. 3.9 shows the opening, closing, and HI output pressures found from the pressure transfer curves by carrying out a sensitivity analysis on four design parameters. A nominal value of 0.41 MPa/mm^3 was selected for C and 0.635 mm was selected for h. These values were chosen to correspond closely with the experimental valve model described in the next section.

The sensitivity analysis shows that an initial increase in the valve seat height decreases the valve closing pressure below the HI output pressure. However, increasing the valve seat height too much results in the opening pressure dropping below the low system pressure P_{low}. This indicates that a larger increase in valve seat height would

need to be accompanied by a increase in system high pressure to ensure desired valve function.

The sensitivity analysis also shows that area fraction has no effect on closing pressure, but has a positive linear effect on valve opening pressure. This suggests that it might be an important design parameter for changing the hysteresis behavior of the valve without affecting the valve closing pressure. For a sufficient positive valve seat height, the closing pressure would still be constant for increasing area fraction, but would be below the HI output pressure. An increase in area fraction might reduce the difference between opening and closing pressures while maintaining a constant valve closing pressure.

The membrane stiffness has an equivalent linear effect on both the valve opening and closing pressures. For a positive valve seat height, the effective stiffness acts as a gain parameter, magnifying the effect of the seat height. As such, it might a useful design parameter for decreasing the valve thresholds for a given valve seat height.

Increasing the relative resistance in the sensitivity analysis for no valve seat height leads to valve closing pressures that come close to the HI output pressures. Additionally, the resistance has no affect on valve opening pressure. This analysis is interesting from a design perspective because the relative resistance is not related to the valve geometry or material properties. Therefore, key features of the valve performance are dependent on circuit design. An additional point to consider is that relative resistances play an important role in circuit dynamics. Increasing the pull-down resistance causes the output pressure to take longer to drop to a LO pressure once the vale closes. Similarly, increasing valve resistance causes the output pressure to take longer to achieve a HI state once the valve opens. I will elaborate more in the next chapter on resistance of circuit elements and their effect on the dynamic performance of logic circuits.

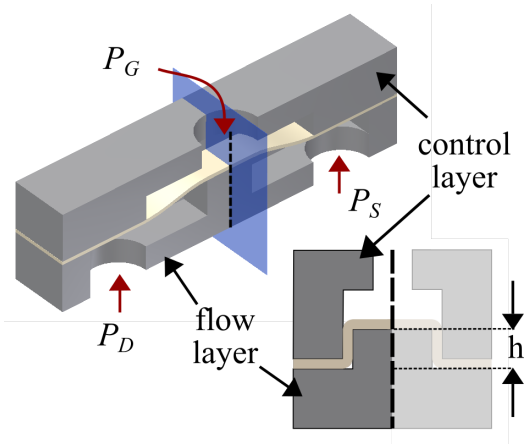

(a)

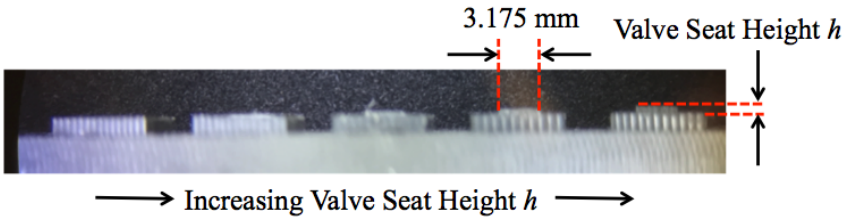

(b)

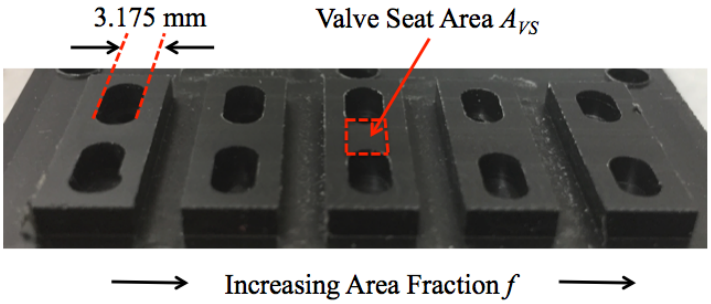

(c)

Figure 3.10: (a) A CAD model of the fabricated pressure-gain valve in a closed state. (b) A side-view of five experimental valve seat heights fabricated out of Delrin with increasing height from left to right. (c) An image of five experimental valves fabricated out of Delrin with decreasing area fraction from left to right.

3.4.2 Macroscale Experimental Validation

To support the analysis with the mechanistic model, macro-scale fluidic valves were fabricated and tested in experiments designed to explore the dependence of

valve operation on certain design parameters.

3.4.2.1 Experimental Setup

The gate and flow layers of the valves were machined out of 12.7 mm Delrin and bolted together with a latex sheet (Latex Rubber, 0.254 mm Thick, McMaster-Carr) sandwiched between them. Fig. 3.10a shows two cross-sections of the CAD design for the valve assembly. The control layer was a rectangular cavity with a length of 7.62 mm and a width of 3.175 mm. Five flow layers were fabricated, all with area fractions of 0.15, but varying valve seat height from 0 to 0.635 mm in increments of 0.127 mm. The flow layer of the valves is pictured in Fig. 3.10b. Five more flow layers were fabricated with no valve seat height ($h = 0$), but with varying area fractions. The flow layer of the fabricated valves is pictured in Fig. 3.10c. The widths of all valve flow channels were made to be 3.175 mm to match the width of the control layer cavities. In varying the seat height in the flow layer, the width of the added height was made 0.254 mm thinner than the width of the channel. This allowed the control and flow layers to fit together and the membrane to seal the channel along the side of the added height (see Fig. 3.10a on the right).

The valves were individually tested by arranging them in a pneumatic NOT gate setup. For each test, the valve gate G was connected to a precision electronic pressure regulator (VSO-EP 990-005003-015, Parker Hannifin Corp.) that provided pressure between 0 and 100 kPag. The drain D of the valve was connected to an 80 kPag pressure supply, serving as the high pressure P_{high}. The source S of the valve was split into two. One part was connected through a length of thin tubing (Miniature Clear EVA tubing, .02" ID, McMaster-Carr) to atmospheric pressure (0 kPag), serving as the system low pressure P_{low}. The other was connected to a pressure transducer (PX40-100G5V, Omega Engineering Inc.), serving as the system output pressure P_{out}. The pressure transducer measured the output pressure P_{out} of the NOT gate as the

input pressure P_{in} was varied using the pressure regulator.

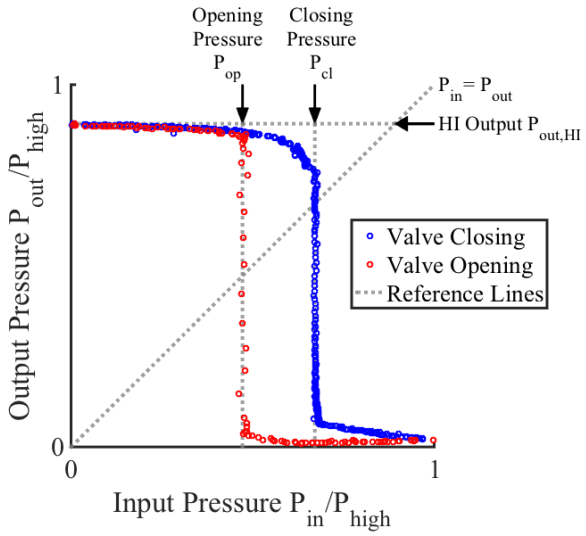

Figure 3.11: Sample data used to find opening and closing pressures with annotated data values from the input and output of the fluidic NOT gate.

3.4.2.2 Experimental Results

To determine the valve opening and closing pressures, we analyzed the pressure input versus output data. Fig 3.11 shows the pressure input plotted against the pressure output for one valve configuration. The valve closing pressure was found as the input pressure (when increasing) at which the output pressure dropped to within 25% of the low source pressure, which in this case is atmospheric pressure. The opening pressure was taken to be the input pressure (when decreasing) at which point the output pressure rose to 75% of the final HI output pressure.

The results for the experimental valves are shown in Fig. 3.12. Results in Fig. 3.12a show that increasing the membrane pre-load results in lower valve closing and opening pressures, with the three most pre-loaded cases exhibiting output pressures sufficient for control of a subsequent inverter circuit (less than $P_{out,HI}$). The results for the closing and opening pressures agree with the general trend of the mechanistic model. In particular, we see that with no pre-load, the valve is not cascadable with an output

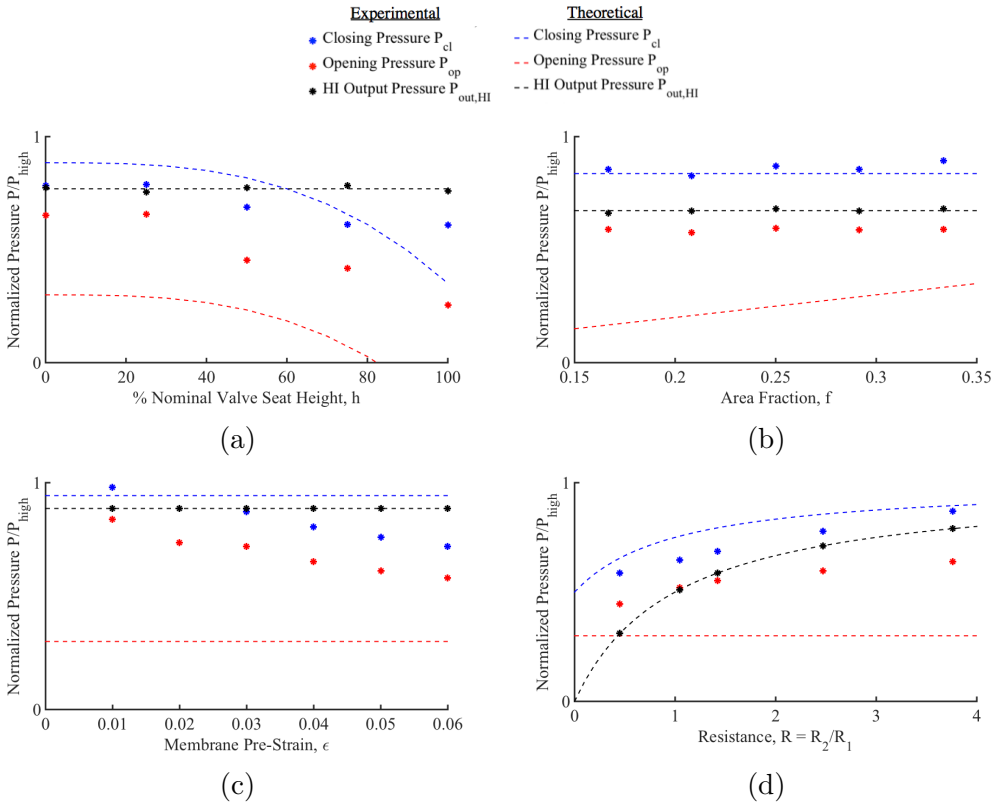

Figure 3.12: (a) Results for five valve seat heights with increasing height corresponding to more pre-load on the membrane. (b) Results for five area fractions with no pre-load. (c) Results for five pre-strained membranes with valve no pre-load and constant area fraction. (d) Results for five pull-down resistances with constant area fraction and no pre-load.

pressure lower than the valve closing pressure. However, as the pre-load is increased, the closing pressure becomes less than the inverter output pressure. Fig. 3.12b shows the valve opening and closing pressures for five different area fractions. The opening and closing pressures remain constant for varying area fractions. Fig. 3.12c shows results for straining to the membrane prior to clamping it between the top and bottom plates. Fig. 3.12d shows results for varying the pull-down resistance R_2 in the experimental inverter circuit, corresponding to varying parameter R.

3.5 Discussion

Our experimental results contribute to the validation of a mechanistic rigid plate model of the elastic membrane fluidic valve. Increasing pre-load on the membrane resulted in valve closing pressures below the HI output pressure of the fluidic inverter. Thus, the HI output pressure would be strong enough to close another fluidic valve supplied with the same system pressures. The closing pressure threshold below the HI output pressure enables the valve to overcome the pressure loss due to the relative resistance of the valve. For the area fraction experiment, the results for the closing pressures follows the mechanistic model well; the closing pressures remain constant with varying area fraction. The circuits are thus not cascadable. Unlike the model, the opening pressure remains unchanged for varying area fractions. Straining the membrane prior to clamping introduces a tensile residual stress that has a linear interrelationship between pressure drop and membrane deflection [61, p. 38]. While not related directly to the C parameter described in the model, the linear effect on the membrane behavior is similar and thus pertinent to the model validation. A similar trend can be seen in the pre-strain results and the sensitivity analysis for parameter C.

The results for the relative resistance R agree with the HI output pressure and closing pressure trends captured by the mechanistic model well. In particular, as relative resistance increases, both the HI output pressure and the closing pressure increases, but notably the two pressures get closer to one another. Increasing resistance causes the opening pressure to increase, but does not follow the trend predicted by the model

The LO output was also sufficiently low in all cases to act as a logical LO input for a subsequent inverter circuit. All the valves also exhibited hysteresis in that the opening and closing pressures were different for each valve, which agrees with the mechanistic valve model.

The mechanistic model was not predictive of the relationship between design parameters and opening pressures. The membrane used in the experiment was thin

relative to the size of the valve, with a thickness to edge length ratio of 0.08, so the rigid plate approximation does not capture its behavior well. However, a similar design parameter was shown to affect opening and closing pressures in work done by Rhee et al. [51]. A possible reason for this might be that a smaller area ratio would result in larger valve resistances due to an increase in the length of the constriction that forms between the valve seat and the membrane. As described above, the model predicts that increasing the valve resistance would affect the opening and closing pressure of the valve. Further, as the valve gate pressure increases, the effective size of the channel between the membrane and the valve seat gets smaller. A smaller channel leads to an increase in the valve resistance, which might result in a valve closing pressure that is below the largest HI output pressure without the need for pre-load. The addition of the dependency of valve resistance on area fraction to the mechanistic model would then suggest that resistance and area fraction are key design parameters for achieving cascadability without pre-load.

Many groups have reported that the source of hysteresis in fluidic valves is the valve membrane sticking to the valve seat when in a closed state [65, 11, 28, 62, 29]. The results of the experiment suggest that sticking between membrane and valve seat may not be the only source of hysteresis. The latex used in the experiment was powdered, reducing the stickiness of the material, so that the contact between the membrane and valve seat (Delrin) was not noticeably sticky. However, results showed hysteresis in all cases.

An interesting effect of adding pre-load is that for the valve to function, the pressure applied at the drain must overcome the forces due to the pre-load. This phenomenon relates to the sensitivity analysis of the valve seat height in Sec. 3.4.1. A large valve seat height drives the opening pressure below the system-wide low pressure P_{low}. The opening pressure, found from Eq. 3.7, still depends on the area fraction, but when there is no pressure applied at the gate, the system high pressure

P_{high} at the drain must overcome the membrane stiffness to enable fluid flow. This phenomenon is referred to as the *breakthrough pressure* in the pressure-based design described by Devaraju et al. [14]. For a given system pressure, it is important to maintain an opening pressure above P_{low} to enable a valid LO logical state.

The valve model does not incorporate a change in resistance of the valve as the gate pressure is increased, which might play a significant role in achieving cascadability. The analysis of sensitivity indicates increasing relative resistance corresponds to an increase in HI output pressure, but is not sufficient for achieving a closing pressure beneath the HI output pressure. However, the model gives an intuitive understanding of how an active change in valve resistance due to gate pressure might aid in attaining closing pressures below the HI output pressure without pre-load. From Eq. 3.2 in the model, the HI output pressure decreases as the valve resistance increases and from Eq. 3.8, a decrease in the HI output pressure results in a decrease in closing pressure. A bend or "knee" in the pressure transfer curve as the input pressure approaches the closing pressure can be seen in Fig. 3.11, which can be attributed to an increase in the valve resistance as the input pressure at the valve gate increases. When the valve is fully open, there is a maximum HI output pressure, but as the valve begins to close, the HI output pressure decreases, as seen in the "knee" in the transfer curve. Thus, a valve closing pressure below the maximum HI output pressure might be achieved by this effect without the need for pre-load. Experimental results shown in Fig. 3.12c show closing pressures below the HI output pressure without any valve seat height. These results suggest that valve gate pressure causes a more rapid increase ("sharper knee") in valve resistance for stiffer membranes. It is possible that this phenomenon is the means by which the standard vacuum-based valves achieve cascadability without pre-load, but further analysis is required to confirm this. The "knee" in the pressure transfer curve is not predicted by the model, but will be of high interest in the next chapter. I will further elaborate on the effect of gate pressure on valve resistance and

expand the analysis to the dynamic behavior of logic circuits.

With a fluidic valve that enables cascadability, it becomes possible to make more complex logic circuits that enable the creation of latching circuitry. Placing two valves in series with a line resistance results in a NAND gate, wherein the output is HI only when both inputs are LO. One form of a D flip-flop can be created using four NAND gates and one NOT gates (9 total valves). The function of the D flip-flop is to hold a pressure-state after the input is removed. As such, it is able to serve as a basic addressable memory unit. Arranging D flip-flops in a series enables the creation of a shift register, where the pressure-output of each flip-flop addresses a pneumatic actuator and a subsequent flip-flop. A shift register addressing a row of actuators of arbitrary length can be controlled serially with just two external control features - a clock signal and a data signal. The flip-flops can also be implemented in a matrix in similar fashion to the construction of thin-film transistors in active matrix LCD screens, as described in Sec. 3.1. The actuators can then be addressed in an X-Y matrix using pneumatic flip-flops, allowing for many haptic features to be controlled with only a few external control lines. Cascadable fluidic logic coupled with pneumatic actuators would enable the creation of a large display that could have commercial applicability for electronic braille devices and be used for novel surface haptics experiments involving human subjects that combines tactile graphics with braille.

3.6 Conclusions

This chapter presented a mechanistic model of a fluidic valve that can be used to determine how certain design parameters affect the ability of fluidic circuits to achieve cascadability in digital logic circuits. Very few parametrized models capable of informing valve designs have appeared in the literature. Moreover, debate still exists around general behaviors exhibited by fluidic valves that contribute to cascadability.

No model has combined the mechanisms of pre-load, area ratio, effective membrane stiffness, and valve resistance. Experimental results from a macro-scale realization of the fluidic valve support the model's use for analyzing the sensitivity of closing pressure to pre-load, circuit resistances, and membrane stiffness or pre-strain. As discussed, experimental results also support the idea that including the dependency of the valve resistance on gate pressure might improve the model's predictive ability, particularly for the sensitivity of cascadability features to area fraction and resistance. The model developed in this chapter represents a useful tool for designing microfluidic fluidic valves for cascadable logic circuits.

CHAPTER IV

Modeling Latching Fluidic Circuits to Determine Clocking Limits for a Refreshable Braille Display

4.1 Introduction

Refreshable braille displays (RBD) raise and lower dots on a surface under computer control, making digital media accessible to braille readers. The speed with which an RBD can refresh characters is a design requirement that depends somewhat on how a given RBD is used. Single line commercial RBDs achieve refresh rates around 10 Hz and a rate on the order of 1 Hz is tolerable for multiple-line displays [56]. Current commercial RBDs are based on piezoelectric technology; while capable of fast refresh rates, the technology is bulky and expensive, limiting the practical size of displays to a single line. We are pursuing technology that would enable the creation of a full-page RBD capable of rendering both braille text and tactile graphics in a large format. Pneumatic actuators are a promising technology for creating a full-page low-cost RBD. They meet the force, deflection, and spacing specifications for braille [58]. Previously, the need for an external control feature (electronic valve) for each actuator stymied the use of pneumatic actuators in large-array tactile devices.

In Chapter III (also published in [59]), a method for controlling pneumatic actuators with integrated fluidic logic networks was introduced, wherein each actuator is

addressed by a fluidic latching memory unit. In analogy to electronic memory devices, pressure-encoded signals (high and low pressure) can be sequentially written and stored in a pneumatic memory circuit using a pressure-based clock pulse. As in computer screens, tactile pixels (taxels) are addressed using sequential logic circuits and an associated clock signal to enable updates on a RBD. The number of external electronic control valves can be reduced by several orders of magnitude, resulting in a highly scalable and manufacturable RBD.

The previous chapter in this thesis describes a key component of the enabling technology for integrating pneumatic actuators with fluidic logic for RBDs. In this chapter, attention is paid to enabling the highest possible RBD refresh rates. As an example, in a basic fluidic shift register design, two external electronic control valves can address any number of actuators or dots using integrated logic. A data signal controls the pressure-encoded information and a clock signal controls the information input speed.

The duration of the clock pulse must exceed a minimum value to ensure information is not corrupted as it is passed along a shift register. When a clock input is enabled, pressure-based information passes as an input into a logic gate. Each logic gate has a propagation delay associated with the time it takes for the output to reach a correct, stable condition, given an input. Therefore, pressure-encoded 1s and 0s must be given time to settle before they are shifted to the next node (before the next clock pulse). If a new clock pulse or input appears too quickly, the previous input may be lost, resulting in the propagation of incorrect outputs. As the number of actuators arrayed along a shift register increases, the refresh rate of the whole display decreases. A typical full page of braille has 25 lines with up to 40 cells per line, where each cell consists of 8 braille dots (4x2). Therefore, a 100 by 80 grid of actuators (8000 total dots) would form a full-page RBD. If 160 external electronic control valves are available (clock and data for each column of dots), a clock frequency of 100 Hz is required

to produce in a full-page refresh rate of 1 Hz. In summary, the propagation delay of circuit elements limits the clock frequency that can be used to correctly control logic circuits. Therefore, understanding the behavior of circuit elements - particularly how pressure builds up *over time* to achieve correct logic states - is critical for achieving fast refresh rates for pneumatic RBDs.

There has recently been a push toward realizing pneumatic logic circuits with high operational speeds in the field of microfluidics, but analytical treatments of the factors that contribute to the time-dependent behavior of these circuits have not appeared in the literature to date. For microfluidic applications requiring high operational speeds, pneumatic circuits are typically preferred over hydraulic circuits due to the much lower viscosity of air leading to higher possible speeds [14]. Grover et al. [22] reported pneumatic circuit control with pressure pulses of 80 ms, but noted occasional failure of the circuits due to "timing errors". Jensen et al. [30] reported circuits controlled with 500 ms pulses, but cited a need for further characterization of airflow through pneumatic circuits to improve response times. Weaver et al. [76] and Burns et al. [51] report speeds of pneumatic logic circuits on the order of 0.5 Hz and suggest that using positive pressure sources and scaling the size of circuits might lead to faster response times. Devaraju et al. [14] reported an increase speed of up to 10 Hz by using positive-pressure logic circuits and Duncan et al. [15] later reported ring oscillator and 8-bit counter frequencies of 22.1 Hz and 6 Hz, respectively, by scaling down negative-pressure logic circuits.

With the exception of Duncan et al., who in a follow-up paper to [15] developed an analytical model for the dynamics of oscillator circuits [16], none of these groups analyzed the time-dependent behavior of the circuits or what gives rise to the "timing errors" that affect circuit behavior. A suitable analysis (and accompanying model must consider the dynamics of continuous states that arise because of parasitic phenomena. The so-called "timing errors" arise because the order in which multiple

threshold crossings occur must not be violated to ensure function. Analyses considering continuous states of pneumatic circuits have not appeared in the literature to date, with a singular exception of Duncan et al. [16]. Duncan et al., however, only analyzed an oscillator circuit, and did not consider more complex bistable pneumatic circuits with inputs. I call a model and accompanying analysis that lacks continuous states a "switch-level" model. Continuous pressure signals are approximated as discrete binary states; such a model is useful for understanding basic function of circuits, but does not consider input timing constraints and time-dependent signal transfers that affect the validity of applied signals. Further, no one to date has analyzed the time-dependent behavior of more complex bistable pneumatic circuits capable of memory storage, which are required for application of the technology for RBDs. The behavior of bistable logic circuits is defined by *feedback loops* that take time to reach a stable state based on the timing of inputs, e.g. clock signals. While the time-dependent behavior of bistable circuits in electronics has been studied in depth [74], the compressibility of air and the hysteretic behavior of the fluidic valves (fluid transistors) both contribute to nonlinear pneumatic circuit dynamics. In particular, fluidic valve behavior [63, 64] and the effect of compressibility of air on pneumatic circuits [16] have been studied in the microfluidics domain, but characterization of airflow through bistable microvalve networks has not been studied to date. This chapter presents a first-principles hybrid automaton model suitable for analyzing the time-dependent behavior of bistable pneumatic circuits. The new model incorporates the compressibility of airflow, the hysteretic behavior of microvalves, and the dependence of valve resistance on control pressures. A model-based simulation and a microfluidic realization of a pneumatic memory circuit are presented that investigate the effects of input timing parameters of circuit response times.

The remainder of this chapter is organized as follows. Section 4.2 describes the function of fluidic valves and basic logic circuits. Concepts and terms important in

modeling the dynamics of pneumatic logic circuits are introduced and described. In Section 4.3, a first-principles model of the fluidic valve as a variable resistance is introduced and a hybrid automaton model of a pneumatic memory circuit is developed that combines discrete and continuous states. Section 4.4 compares simulation results of the hybrid automaton model outfitted with the fluidic valve resistance model and with a switch-level valve model. An experimental pneumatic memory circuit is fabricated and used to validate aspects of the hybrid automaton model. System identification is used on the experimental circuit to fit parameters of the first-principles valve model. Section 4.5 describes key findings from the model analysis and experimental results that contribute to validation of the model. Section 4.6 summarizes and concludes.

4.2 Basic Pneumatic Memory Unit

A full analysis of pneumatic logic circuits capable of storing binary pressures must consider both discrete and continuous dynamics. Using pressure-controlled fluidic valves that function in analogy to electronic transistors, binary states at certain nodes within a fluid circuit are delineated by thresholds above which pressure is considered logical HI and another threshold below which pressure is considered logical LO. Using resistive fluid lines (or constrictions) and pressure-controlled fluidic valves, fluid circuits can be created that operate in complete analogy to electronic circuits based on resistor-transistor logic (RTL). Pressure states at circuit nodes are determined by fluid flow and relative resistances. HI output pressure states develop when fluid flow causes pressure to build up at one end of a resistance. LO output pressure states occur when there is no steady-state fluid flow and the output is effectively connected to ground resulting in no pressure buildup at the output.

When considering the operation of memory circuits at high-speed, there exist timing races that give rise to unwanted circuit behavior. Bistable circuits must be

given sufficient time to reach a desired state once an input is applied. If an input is removed too quickly, the bistable circuit may not function as desired. In the following subsection, the behaviors of key components for creating pneumatic memory circuits are discussed: (1) a pressure-controlled fluidic valve, (2) a simple single-valve logic gate, and (3) a basic pneumatic memory storage unit, the D latch. In particular, we discuss the characterization of the continuous dynamics of these that enable a full analysis of function for essential components in a pneumatic memory circuit.

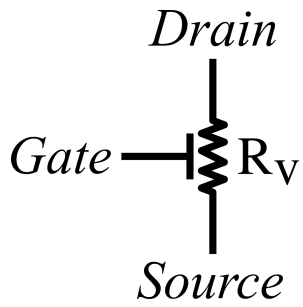

Figure 4.1: In analogy to the electronic transistor, the pressure at the gate G controls the flow between the drain D and source S of the valve. When fluid is flowing (open valve), the valve acts as a fluidic resistor with resistance R_v. When closed, the resistance of the valve is considered infinite, allowing no airflow.

4.2.1 Pressure-Controlled Fluidic Valve

The pressure-controlled fluidic valve uses binary pressure signals to control fluid flow and as such, is an essential component in fluidic logic circuits. The fluidic valve can be described as having two distinct states, open and closed, which is analogous to an electronic transistor. The states are defined by distinct opening and closing pressure thresholds that vary based on valve design. Cascaded logic gates built with fluidic valves have demonstrated nonlinear gain and valid switching thresholds that enable digital abstraction [51, 16, 14]. In analogy to the three-terminal electronic metal oxide semiconductor field effect transistor (MOSFET), pressure at fluidic valve gate terminals control fluid flow between the drain and source terminals. In terms of positive logic, a HI (1) gate pressure closes the valve, cutting off fluid flow, and a LO

(0) pressure opens the valve, allowing fluid flow. The fluidic valve can be considered a pressure-controlled current source or resistance [63]. Fig. 4.1 shows the symbol used to represent the fluidic valve in this chapter.

Discrete models of the valve using pressure thresholds to distinguish between valve states have been used previously to characterize behavior of hydraulic and pneumatic circuits [45, 16]. In these models, the dynamics of the fluidic valve are considered discrete; the valve snaps open or closed quickly when pressure thresholds are crossed, creating two distinct valve states. However, for pneumatic circuits in which fluidic valves are opening and closing pressurized flow at finite rates, the transient behavior of the valves influences the circuit dynamics to a greater degree. In particular, the equivalent resistance of the valve may be affected by the gate pressure. In previous work characterizing the performance of elastomer-based microvalves [59, 51], the existence of regions of negative gain in logic gate transfer functions suggests that valve resistance is not constant in the time period leading up to valve closing. The dependence of valve resistance on gate pressure is non-trivial. Discrete models of the valve do not capture these regions of increased valve resistance that may play a significant role in circuit dynamics.

For a constant gate pressure, the valve resistance depends on the pressure differential across the valve. For hydraulic systems, flow resistance is relatively constant for laminar flow conditions and can be approximated using the Hagen-Poiseuille formula [47]. Due to the small channel dimensions in microfluidics, the Reynolds number for both hydraulic and pneumatic flow is usually much less than 100, well below the approximate Reynolds number for transition to turbulent flow of 2000 [16, 3]. However, in pneumatic systems, airflow resistance for laminar flow varies based on the pressure differential across a restriction [49, p.334]. While a correction factor for Poiseuille's equation can be applied for compressible flow, it is only valid for small pressure differences. However, large pressure differences develop within the circuit when valves

open and close. In modeling steady-state circuit behavior, the relative resistance of circuit elements in RTL logic ensures valid logic outputs. Under large pressure differentials, airflow resistance can vary significantly, which leads to non-trivial effects on the transient behavior of the system.

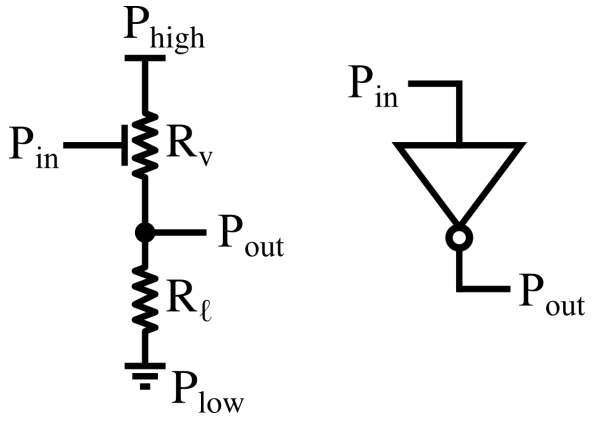

Figure 4.2: Comprised of a transistor and a resistor in series, the NOT gate produces an output pressure signal that is the inverse of its input. On the left, a circuit-level representation. On the right, a symbol used to represent the logic gate.

4.2.2 NOT Gate

Basic logic gates comprised of resistors and fluidic valves function based on the time-dependent buildup of pressure that takes place at certain nodes when valve flow conditions change. The most basic logic gate is the NOT gate (inverter), which in resistor-transistor logic is constructed by placing a fluidic valve and pull-down resistor in series between high (P_{high}) and low (P_{low}) pressure sources, as shown in Fig. 4.2. The function of the NOT gate is to produce an output signal that is the inverse of the input. The circuit is designed such that the valve resistance R_v is smaller than the pull-down resistance R_ℓ. When the gate is open (P_{in} = LO), fluid flows and the difference in resistances results in a pressure buildup at the output that is close to P_{high}, which is a logical HI (P_{out} = HI). When the gate is closed (P_{in} = HI), the output pressure decays over time to P_{low}, which is logical LO (P_{out} = LO). Changes in the valve state cause pressure at the output to change over time by virtue of finite

Table 4.1: Pressure input P_{data} changes the state of the flip-flop outputs P_Q and $P_{\bar{Q}}$ only when the the gate is open ($P_{clk} = 0$).

P_{data}	P_{clk}	P_Q	$P_{\bar{Q}}$	STATE
1	1	1	0	LATCHED
1	0	1	0	—
0	0	0	1	—
0	1	0	1	LATCHED
1	1	0	1	LATCHED

amounts of pressurized air flowing through airflow resistances in the circuit. Air flows to the output from the high pressure source across the valve resistance or from the output to the low pressure source through the pull-down resistance.

4.2.3 The D Latch Memory Circuit

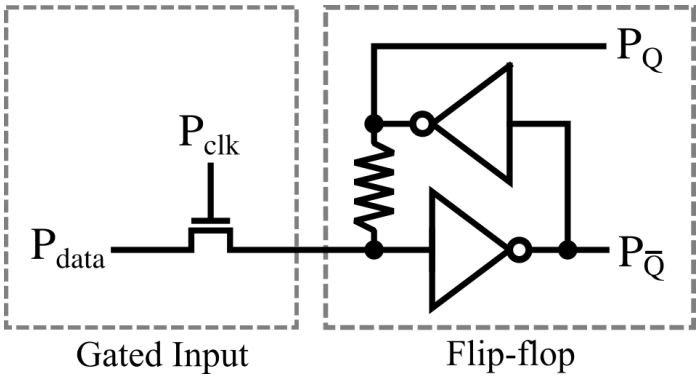

Figure 4.3: A) Comprised of a flip-flop and gated input, the D latch uses two inputs to produce latching memory outputs.

The D latch is a memory circuit that consists of two elements: a bistable flip-flop and a gated input having a clock signal that controls the transfer of a data signal into the flip-flop. The flip-flop is a bistable element, consisting of two NOT gates connected in a *feedback loop* (see right dashed-line box in Fig. 4.3. Once the output of one NOT gate settles to a certain pressure level, the state of the flip-flop is latched and stable. As such, flip-flops are useful in fluidic logic circuits as basic memory elements. The gated input element (left dashed-line box in Fig. 4.3 is used to control the state of the

flip-flop. When the gate is open, the data input is applied to the flip-flop. An added resistance in the flip-flop feedback loop prevents conflict between a new signal from the gated input and the previous flip-flop state. The D latch has two pressure inputs, P_{data} and P_{clk}, and two latching outputs, the buffered output P_Q and the inverted output $P_{\bar{Q}}$. Table 4.1 gives a truth table for the operation of this circuit using a discrete switch-level interpretation. Assuming the pressure values at the nodes are well-defined logical states, the flip-flop has two possible states. When the gate control pressure P_{clk} is LO (0), the fluidic valve is open and the latch input signal, defined here as P_{data}, is able to forcibly change the state of the flip-flop. Pressure evolves in the flip-flop circuit over time until P_Q and $P_{\bar{Q}}$ reach the buffered and inverted logical equivalent of P_{data}, respectively. The truth table gives an intuitive understanding of how the circuit works, but does not consider the continuous dynamics that affect circuit behavior.

For the D latch, the period of time it takes for the output to reach a stable, correct state is called the propagation delay. Once the propagation delay has elapsed after a change in an input, the gate control pressure Pclk can be turned HI (1), latching the flip-flop such that the output pressures P_Q and $P_{\bar{Q}}$ remain unchanged until the gate is reopened. If the gate is latched before the propagation delay time, the circuit does not function correctly. We now seek to understand how the combination of the evolution of pressures and the switching of valves within the D latch circuit determines the propagation delay.

When controlling bistable circuits at high operational input speeds, the timing of inputs affects the behavior of the circuit [41, 35]. The duration and timing of inputs has a non-trivial effect on propagation delay. Marginal triggering can occur in which the circuit operates in a metastable region, having an undefined logical state, for a period of time after an input is initially applied [32]. Under marginal triggering conditions, as the duration of inputs is reduced, after a point, the reduction in input

duration leads to rapid increases in circuit propagation delay and eventual failure [17]. Understanding the behavior of pneumatic circuits under these marginal triggering conditions will allow for precise optimization of device design and time-dependent inputs for increasing circuit speeds.

4.3 Bistable Memory Circuit Model Description

In this work, a bistable D latch circuit is considered that can be implemented in sequential logic circuits for static memory storage. As such, its behavior exemplifies some of the time-related issues that arise in high-speed pneumatic memory circuits.

4.3.1 Assumptions

In the model, the volume of the fluid elements is assumed to be constant. Thus, expansion of air-filled chambers and volume change as a result of valve membrane deflection is not considered. All air-flow is considered laminar, which is valid due to approximate Reynolds numbers well below 2000 for microfluidic circuits [16]. Air compression is considered as an isothermal process (polytropic index n = 1), in which the ideal gas law applies. Air is assumed as having a constant viscosity for the range of pressures used. The effect of air inertance is assumed to be negligible compared to the resistance and capacitance of the system. The volumes at nodes within the circuit are considered non-negligible and constant under variations in pressure.

4.3.2 Fluidic Valve Model

In order to better predict the performance of pneumatic circuits driven at high speeds, a model for the fluidic valve is developed using an analogy to an electronic field effect transistor (FET). Takao et al. developed a model that characterizes the flow-rate characteristics of silicon-based fluidic valves under different pressure conditions [64, 63]. Unlike FETs and the silicon-based valves described by Takao et al.,

elastomer-based microfluidic valves have been shown to have large hysteresis, with separate opening and closing pressures that are dependent on valve design [51, 14, 59]. The model described here considers the valve as a finite state machine with resistance dependent on both the valve gate pressure and the differential pressure across the valve. The resistance is defined as the change in differential pressure required to make a unit change in flow rate ($Pa - s/kg$). When the valve is in an open configuration, the valve membrane is actuated by the pressure at the valve gate P_G. Similar to the operation of a FET, the current in the flow channel for a constant applied drain-source pressure differential is related to the gate pressure P_G. As the gate pressure approaches the valve closing pressure P_{cl}, the resistance increases until the valve closes, shutting off flow between drain and source.

The resistance of a valve is modeled as inversely related to the difference between closing pressure threshold P_{cl} and gate pressure P_G. In addition to the dependence of the resistance on gate pressure, the airflow rate through a flow-restricting element is proportional to the pressure differential between upstream and downstream parts of the element [49]. When the valve is open, the resistance of the valve is related to the pressure difference between the drain and source P_{DS}. The channel resistance of a fluidic valve in the open configuration based on the pressure-dependent relationships described above is expressed by the following empirical relationship:

$$R_{V,op}(P_G, P_{DS}) = \frac{K(P_{DS}/P_{high})^n}{[(P_{cl} - P_G)/P_{cl}]^m} \tag{4.1}$$

where K, m, and n are parameters based on valve design and working fluid conditions, P_{cl} is the valve closing pressure, and P_{high} is the system-wide high gauge pressure. The equation applies to positive pressure circuits in which the valve opens for values of P_G greater than P_{cl}. The values of m and n provide the degree to which the resistance is related to the pressure difference P_{DS} and the gate pressure P_G, respectively.

The parameter K is a gain factor that depends on valve design, material stiffness, and working fluid [63]. The contribution of the gate pressure to valve resistance is normalized with respect to the valve closing pressure and the contribution of differential pressure is normalized with respect to the system-wide high pressure P_{high}.The selection of the parameters is left to be experimentally determined by system identification. To capture the hysteretic behavior, the valve is modeled as a finite state machine, with resistance dependent on valve state - open or closed. When in an open state, the valve closes if the gate pressure rises above the valve closing pressure P_{cl}. Once closed, the valve opens once the gate pressure drops below the valve opening pressure P_{op}. Fig 4.4 shows two finite state machines. The finite state machine on the left represents the valve hysteresis for the gate-pressure dependent model described above. When the valve is open, it is governed by Eq. 4.1 and when it is closed, the resistance is infinite. On the right, a switch-level model is applied that considers the valves as having infinite valve gain at the valve opening and closing pressures (discrete ON/OFF behavior). When the valve is open, the valve resistance is constant up to the closing pressure condition and infinite when the valve is closed. These two models are later compared in simulation.

4.3.3 Modeling the D latch as a Hybrid Automaton

We model the input-controlled bistable D latch circuit as a hybrid automaton, wherein both discrete and continuous elements govern the dynamics of the system [69]. Fig. 4.5 shows a schematic of an analogous electronic circuit. The capacitances represent fixed volumes within the circuit at each node. The capacitance C at the nodes is defined as the change in the mass of air required to make a unit change in pressure (kg/Pa). Resistors represent airflow resistances, including valves, between the fixed volumes at the nodes. The pressures within the fixed volumes at the nodes P_1, P_2, and P_3 change in continuous time based on the configuration of the fluidic

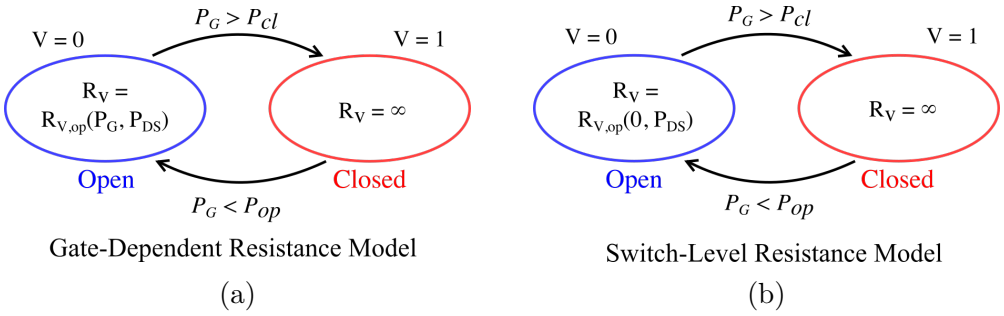

Figure 4.4: The fluidic valve is modeled as a finite state machine. For both the gate-dependent and switch-level models, the switching behavior of the finite state machine is determined by the relationship between the valve gate pressure P_G and the valve opening P_{op} and closing P_{cl} pressures. (a) For the gate-dependent resistance valve model, the resistance in the open condition is found using Eq. 4.1 and varies based on the gate pressure P_G and differential pressure P_{DS}. In the closed configuration, the resistance is infinite. (b) For the switch-level resistance valve model, the resistance in the open state is found using Eq. 4.1 and varies based on only the differential pressure P_{DS}. In the closed configuration, the resistance is infinite.

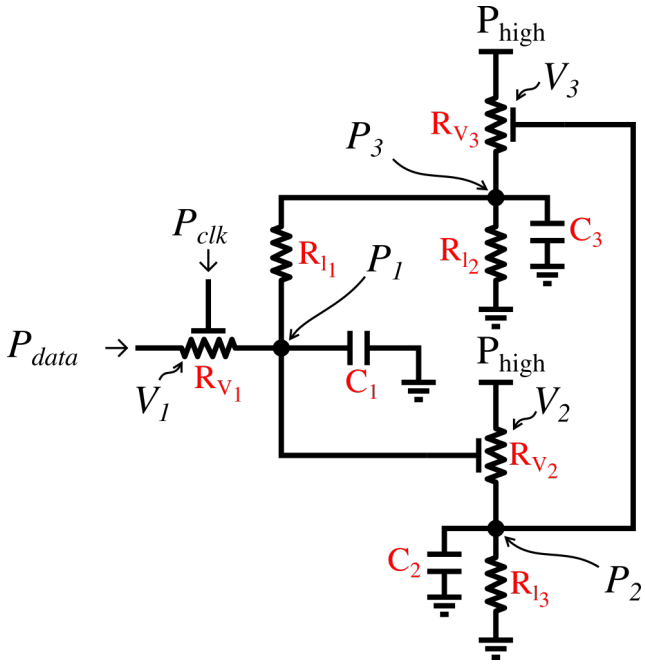

Figure 4.5: The D latch is modeled using an electrical analogy. Capacitors to ground at every node take the place of fluid reservoirs and resistors take the place of fluidic resistors. The inputs to the D latch are P_{clk} and P_{data}.

circuit and they are defined as continuous variables. The valves are represented by binary variables V_1, V_2, and V_3 that take on values based on their behavior as finite state machines as described in Section 4.3.2 and represented in Fig. 4.4. The states

of valves V_1, V_2, and V_3 are determined by valve gate pressures P_{clk}, P_1, and P_2, respectively. Resistance of each valve (R_{V_1}, R_{V_2}, and R_{V_3}) is determined based on the valve state, the gate pressure, and the pressure differential across the valve as detailed in Section 4.3.2.

The other resistances between nodes in the circuit that are not valves (R_{l_1}, R_{l_2}, and R_{l_3}) are modeled based on the dependence of airflow rate through a restriction on the pressure differential across it [49]:

$$R = K_R[(P_u - P_d)/P_{high}]^b, \tag{4.2}$$

where P_u and P_d are the pressures upstream and downstream of the restriction, respectively, K_R and b are parameters related to the geometry of the resistance and working fluid, and P_{high} is the system-wide high pressure. A theoretical determination of the airflow resistance is intractable, but can be determined experimentally. The inputs to the system are P_{data} and P_{clk} that take on values between the system high and low pressures, P_{high} and P_{low}, respectively. The binary valve variables determine the discrete state of the D latch hybrid automaton model that then governs the continuous dynamics of the circuit.

The dynamic equations for the bistable D latch circuit are derived based on the modeling of the valve and restriction resistances described above. The mass flow rate of air $Q(t)$ into a node due to a pressure difference across a resistance connecting to that node is given as:

$$Q(t) = \frac{p_o - p_i}{R}. \tag{4.3}$$

where p_o is the node pressure, p_i is the pressure at a node opposite the resistance, and R is the resistance of the valve or restriction. The dependency of the resistance R on time-dependent pressures within the circuit, outlined in Eq. 4.1 and Eq. 4.2, results in non-linear behavior of airflow. The mass flow rate of air into a node $Q(t)$

Table 4.2: Valve resistance R_V is a function of the gate pressure P_G and differential pressure across the valve P_{DS} ($R_V = f(P_G, P_{DS})$). Gate pressures and differential pressures for the three valves in the D latch model are listed. The valve resistances are then determined by the finite state machine shown in Fig 4.4a and by Eq. 4.1.

	P_G	P_{DS}
R_{V_1}	P_{clk}	$P_{data} - P_1$
R_{V_2}	P_1	$P_{high} - P_2$
R_{V_3}	P_2	$P_{high} - P_3$

is also proportional to the capacitance C and the time-derivative of the pressure at that node $p'_o(t)$, according to the following relationship:

$$Q(t) = Cp'_o(t). \tag{4.4}$$

For a constant volume pressure vessel, applying the ideal gas law results in the following expression:

$$C = \frac{V}{nR_{gas}T}. \tag{4.5}$$

where R_{gas} and T are the specific gas constant and absolute temperature, respectively, and n is the polytropic exponent related to the expansion process.

Referring back to the circuit diagram representation of the D latch in Fig. 4.5, the time-derivatives of the pressures at the nodes in the circuit are found using Kirchoff's law, with pressure analogous to voltage and airflow analogous to current. The D latch model can be outfitted with either the gate-dependent resistance model or the switch-level resistance model. The valve resistances in each case are defined by the finite state machine models shown in Fig. 4.4.

For the gate-dependent resistance valve model, a valve resistance is a function of the gate pressure P_G and differential pressure P_{DS} shown in Table 4.2. For example, the resistance of valve V_1 is based on Eq. 4.1 and is a function of the valve gate pressure P_{clk} and the difference between pressures P_{data} and P_1. The resistance of an

open valve varies with respect to its gate pressure P_G and differential pressure P_{DS}. The resistance of a closed valve is infinite.

For the switch-level resistance valve model, a valve resistance is also a function of the gate pressure P_G and differential pressure P_{DS} shown in Table 4.2. However, the resistance of an open valve does not vary with gate pressure P_G; it only varies with the differential pressure P_{DS}. The resistance of a closed valve is also infinite.

The D latch model results in the following nonlinear continuous dynamics for the system:

$$\dot{P} = \begin{bmatrix} -\frac{1}{C_1}\left(\frac{1}{R_{V_1}}+\frac{1}{R_{l_1}}\right) & 0 & \frac{1}{C_1 R_{l_1}} \\ 0 & -\frac{1}{C_2}\left(\frac{1}{R_{V_2}}+\frac{1}{R_{l_3}}\right) & 0 \\ \frac{1}{C_3 R_{l_1}} & 0 & -\frac{1}{C_3}\left(\frac{1}{R_{l_1}}+\frac{1}{R_{V_3}}+\frac{1}{R_{l_2}}\right) \end{bmatrix} P + \begin{bmatrix} \frac{1}{C_1 R_{V_1}} & 0 \\ 0 & \frac{1}{C_2 R_{V_2}} \\ 0 & \frac{1}{C_3 R_{V_3}} \end{bmatrix} u, \quad (4.6)$$

where P = $[P_1, P_2, P_3]^T$, u = $[P_{data}\ P_{high}]^T$, and the valve resistances (R_{V_1}, R_{V_2}, and R_{V_3}) are defined by the finite state machines shown in Fig. 4.4, based on whether the gate-dependent model or switch-level model is applied. Note that all resistances in the system of differential equations are dependent on continuously-varying pressures, thus the system is nonlinear.

The non-valve resistances (R_{l_1}, R_{l_2}, and R_{l_3}) between nodes are found from Eq. 4.2, respectively. The modeling of valves as finite state machines and the dependence of resistances in the pneumatic circuit on differential pressures at nodes results in a nonlinear hybrid dynamical system. Derivation of the continuous dynamics is relatively straightforward, but a closed-form solution under most conditions is impossible. The results presented in this paper are based on a numerical approximation obtained using a forward Euler numerical integration scheme.

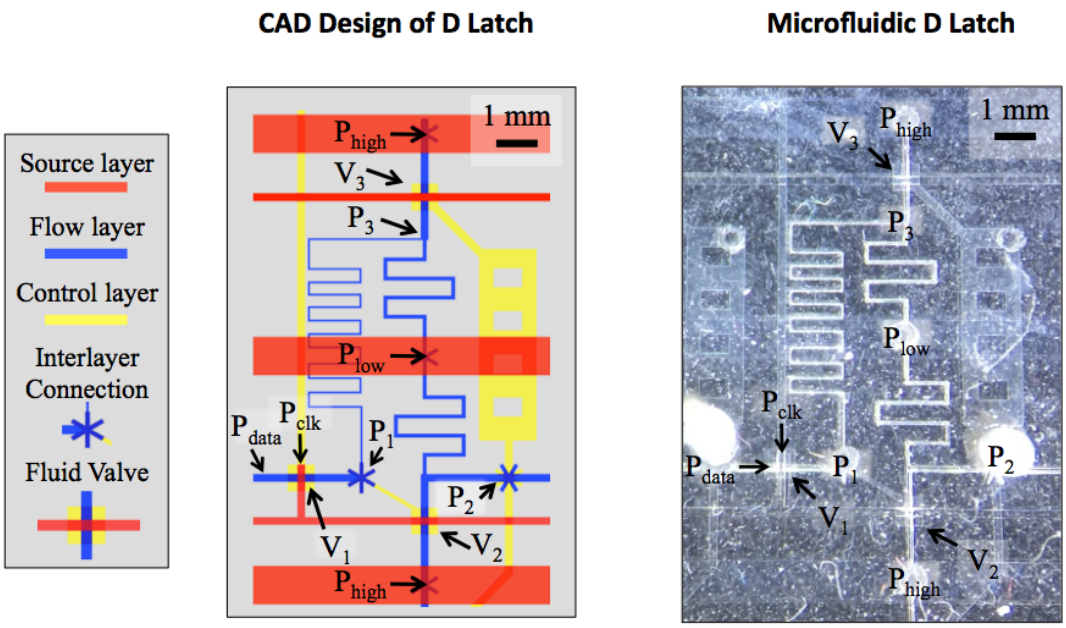

Figure 4.6: A microfluidic D latch circuit was fabricated using three feature layers: the flow layer, the control layer, and the gain layer. Vias were punched through the device to connect the layers in specified locations on the device. Fluidic resistances were formed by winding fluid channels. Connections to the device for pressure inputs and sources were made with elastic tubing.

4.4 Results

The duration and timing of inputs applied to bistable circuits affects their propagation delay. Using the model described above, it is possible to analyze how the propagation delay of the D latch is affected by marginal clock pulse inputs. Here, the effect of the input clock pulse width on the D latch propagation delay for a constant applied data signal P_{data} is analyzed and used to validate aspects of the hybrid automaton model of the D latch. The model can be also be applied in an analysis of other timing parameters related to the data signal such as setup time and hold time, but those are not considered here. A microfluidic D latch circuit was constructed, shown in Fig. 4.6. We used a system identification process to determine resistance parameters from Eq. 4.1 of the microfluidic valves. We then estimated the remaining resistance and capacitance parameters of microfluidic resistances and volumes by fit-

ting the derived governing differential equations to experimental pressure responses. We tested the experimental D latch circuit by applying a range of clock pulse widths for constant HI and LO data inputs. Using the parameters found using system identification, we then tested a range of clock pulse widths in a simulation of the D latch model by applying both the compressible flow valve model and the switch-level valve model and compared the simulation results to experimental results.

4.4.1 Experimental Microfluidic D latch

An experimental D latch device was fabricated using the pressure-based valve design described by Devaraju et al. [14]. Rounded flow channels, essential to valve function, were fabricated by re-flowing patterned SPR-220 on bare silicon wafers [68, 18]. Control and gain layers were fabricated by patterning SU-8 2035 on silicon wafers using standard photolithographic techniques. UV-curable glue (Loctite Light-Activated Adhesive, #3104) was injected into the gain layer and cured under pressure to produce pre-load on the the valve membrane in order to attain desired nonlinear gain behavior, as described by Devaraju et al. [14].

4.4.2 System Identification

We used a system identification process to find the best fit parameters for the valve resistances. A microfluidic NOT gate was fabricated using the same methods and design layout as implemented in the D latch microfluidic circuit. To determine the pressure differential dependence of the valve resistance, a high pressure was applied to one side of the valve while a pressure transducer (Omega, PX40-100G5V) fixed to a known volume was placed to the other side. The gate pressure was set to 0. The pressure response was recorded and the ideal gas law was used to determine the mass flow rate into the known volume, assuming isothermal (polytropic exponent n=1) and the pressure differential curve. Eq. 4.1 was used in curve fitting, with P_G set to

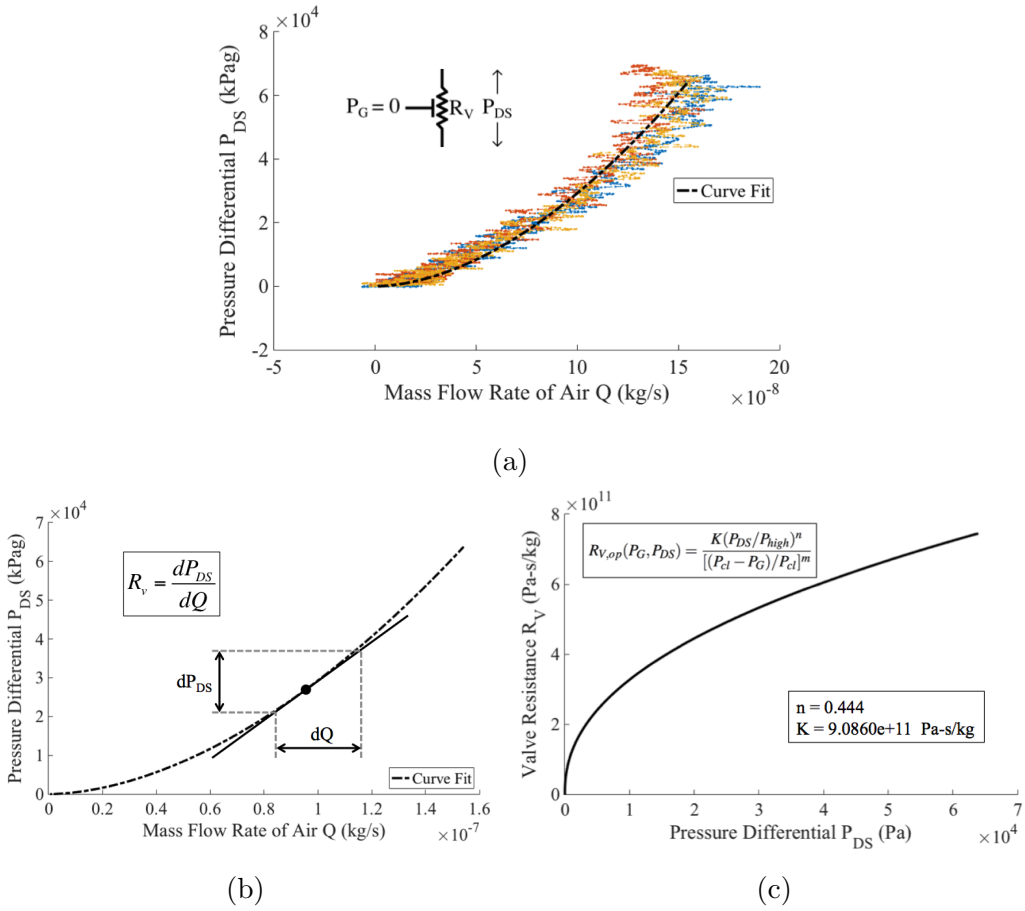

Figure 4.7: System identification was used to determine parameters K and n from Eq. 4.1 for the microvalve implemented in the microfluidic D latch circuit shown in Fig. 4.6. (a) The ideal gas law was used to calculate the mass flow rate of air into a fixed volume at different pressure differentials across the microvalve. (b) A curve was fit to the data, which when differentiated gives the resistance R_V of the valve. (c) The n and K parameters chosen resulted in a flow-pressure-dependent valve resistance governed by Eq. 4.1.

0, to determine parameters related to the effect of pressure differential P_{DS} on valve resistance. Fig 4.7 shows the curve fit to the experimental curves and the resulting parameters selected based on the fit.

Next, we determined the gate pressure dependence of the valve resistance by measuring the pressure transfer curve for the fabricated NOT gate. Fig. 4.8a shows the experimental results for a constant high supply pressure of 100 kPag. The input pressure was varied from 0 to 100 kPag. Eq. 4.1 was used in curve fitting, with P_{DS}

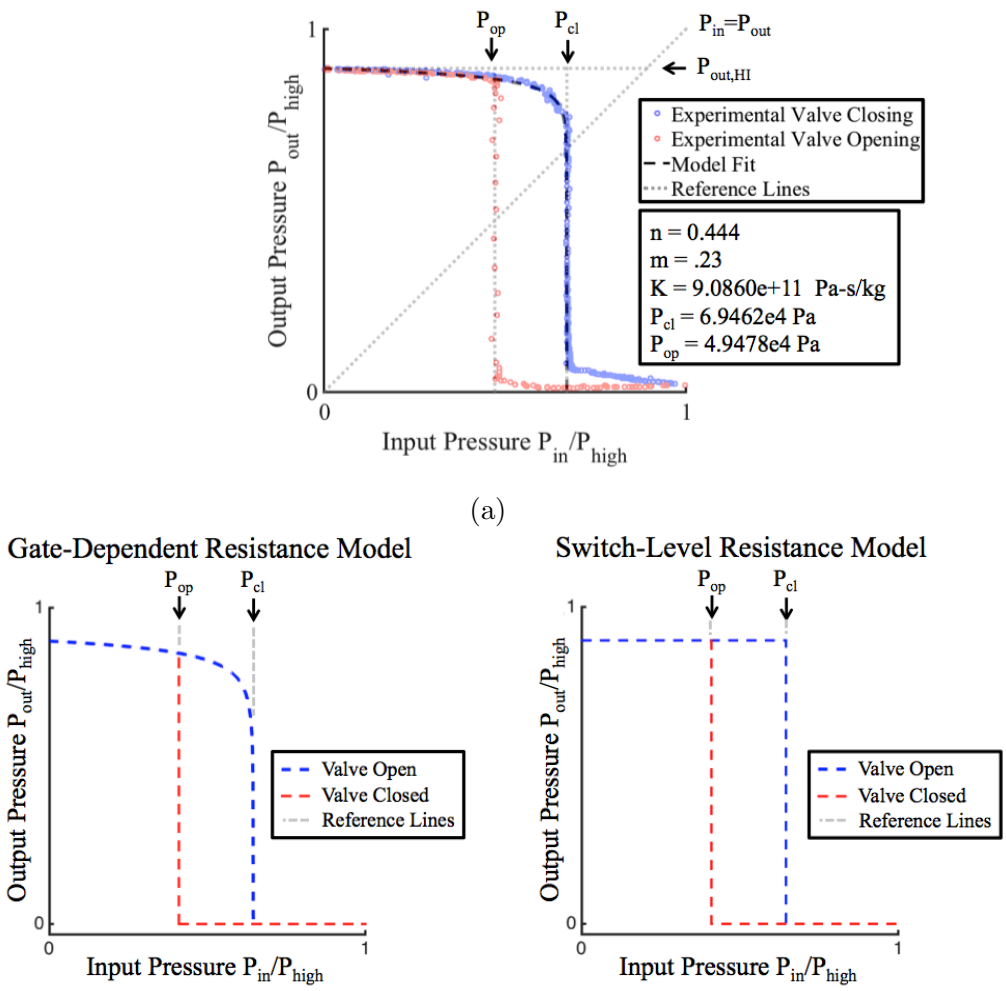

Figure 4.8: (a) A pressure transfer curve is shown for a microvalve implemented in the D latch circuit. System identification was used to determine m, P_{cl}, and P_{op} from Eq. 4.1 for the microvalve implemented in the microfluidic D latch circuit shown in Fig. 4.6. (b) The parameters were applied to the gate-pressure-dependent resistance finite state machine model to arrive at a pressure transfer curve for the valve. (c) The opening and closing pressures were applied to arrive at a pressure transfer curve for a switch-level resistance.

set to the difference between P_{high} and the initial HI output of the NOT gate $P_{out,HI}$. The opening and closing pressures for the valves were determined experimentally by analyzing the pressure transfer curve. The valve closing pressure was taken to be the input pressure at which the output pressure dropped to within 20% of the LO output pressure. The opening pressure was taken to be the input pressure at which

the output pressure rose to 80% of final HI output pressure. The parameters related to the effect of gate pressure P_G on valve resistance were determined from the curve fit and are shown on the right of the Fig. 4.8a. Fig. 4.8b shows the realization of a gate-pressure-dependent model of the microvalve based on the parameters found. Fig. 4.8c shows the realization of a switch-level model of the microvalve based on the parameters found. Note that there is a characteristic "bend" in the gate-pressure-dependent model that is not present in the switch-level model.

The resistance parameters for the built-in resistances were determined experimentally based on a voltage divider interpretation of the fluidic circuit. The output pressure at each node was determined experimentally for a latched (steady-state) D latch by attaching pressure gauges to the microfluidic circuit. Using the valve resistances determined by system identification (described above), the built-in resistances were chosen so that in a simulation of the modeled D latch in a latched state, the node pressures were equal to the pressures found experimentally. Finally, the governing differential equations were populated with the resistance parameters determined above and the capacitance parameters were determined by fitting the model equations to applied step input pressures for fully-opened valves. MATLAB's built-in `fmincon` function was used to minimize the sum of the norm of errors between experimental and theoretical curves to find the best fit.

4.4.3 Experimental Methods

The data and clock inputs to the microfluidic D latch were connected using thin PTFE tubing (PTFE 0.5588 mm ID, Cole-Parmer, EW-06417-21) to electronically-controlled solenoid valves (LHD Series, The Lee Company). The valves were held in a manifold that was maintained at a constant pressure of 100 kPag from an in-house pressure supply. The high pressure input for the device was connected directly to the valve manifold (100 kPag) and the low pressure was kept at atmospheric pressure

(0 kPag). Valves were controlled using an Arduino microprocessor and computer.

Experiments were performed under a stereo microscope and recorded at 960 frames-per-second using a high-speed camera (Sony Cyber-shot RX100) mounted to the microscope eye-piece. Videos were post-processed by examining light reflection within the microfluidic device from a DC ring light source. Prior to each test, the system was programmatically pressurized at evenly spaced pressures between 0 and 100 kPag. Light reflectivity was shown to vary linearly with pressure above 200 kPa at specific nodes within the device. In addition, valve opening and closing could clearly be determined based on distinct changes in brightness of light in the area of valve membranes within the circuit.

For testing, the clock input was kept high initially, keeping valve V_1 closed. Clock pulses were applied by turning the clock input solenoid valve low for a duration of time corresponding to the clock pulse width T. A range of clock pulse widths were applied while recording high speed video of the D latch circuit. Data was collected for high (100 kPag) and low (0 kPag) data inputs, resulting in both HI-LO and LO-HI flip-flop transitions.

4.4.4 Simulation Methods

Using the parameters determined by system identification of the experimental D latch, different pulse widths were applied in simulation to the hybrid automaton D latch model described above. The clock pulse width is defined here as the time between the falling and rising edge of the clock signal. An ideal clock signal represented by a perfect square wave was applied, such that when the D latch clock signal P_{clk} goes from HI to LO, valve V_1 in the D latch opens and the data input P_{data} is connected to the bistable flip-flop through R_{V_1}. When the clock signal goes HI again, valve V_1 closes and the P_{data} input is closed off from the flip-flop. Decreasing pulse widths were applied until the inverted D latch pressure output P_2 did not reach the

desired stable output state. Results for successful D latch transitions are shown in Fig. 4.10 for both the gate-dependent valve model and the switch-level valve model.

4.4.4.1 Experimental and Simulation Results

The continuous-time pressures for the two experiments (based on the approximate linear relationship between light-reflectivity and pressure) are shown in Figure 4.9. Pressures are normalized with respect to their maximum pressure for each trial. The state of valve V_3 is represented as a binary signal. The clock pulse width signals applied to the solenoid valve are shown on the right of the plots. For the LO-HI D latch experiment, clock pulse widths between 22.6 ms and 50 ms were applied. For the HI-LO experiment, clock pulse widths between 20 ms and 50 ms were applied. Propagation delays were calculated in each trial as the difference between the time that the clock signal solenoid valve was activated and the time that valve V_3 changed states, based on light reflection in the valve area. The experimental propagation delays for varying clock pulse widths are shown in Fig. 4.10. The left figure shows HI-LO transition of the valve V_3 and the right shows the LO-HI transition, corresponding HI and LO data inputs, respectively.

The behavior of the hybrid dynamical model in response to decreasing clock pulse widths for the LO data input led to a marked increase in propagation delay for the gate-dependent valve model, but not the switch-level model. Referring to the LO-HI output transition results in Fig. 4.10, the propagation delay for the resistance-dependent valve model is constant when T is large. As T decreases and approaches its minimum value, the propagation delay begins to increase until failure. For the HI-LO simulation, the propagation delay is approximately constant for all clock pulse widths that result in a valid D latch transition. Simulation results are also shown for the hybrid automaton model outfitted with the switch-level valve resistance model. The switch-level model yields a near-constant propagation delay as the clock pulse

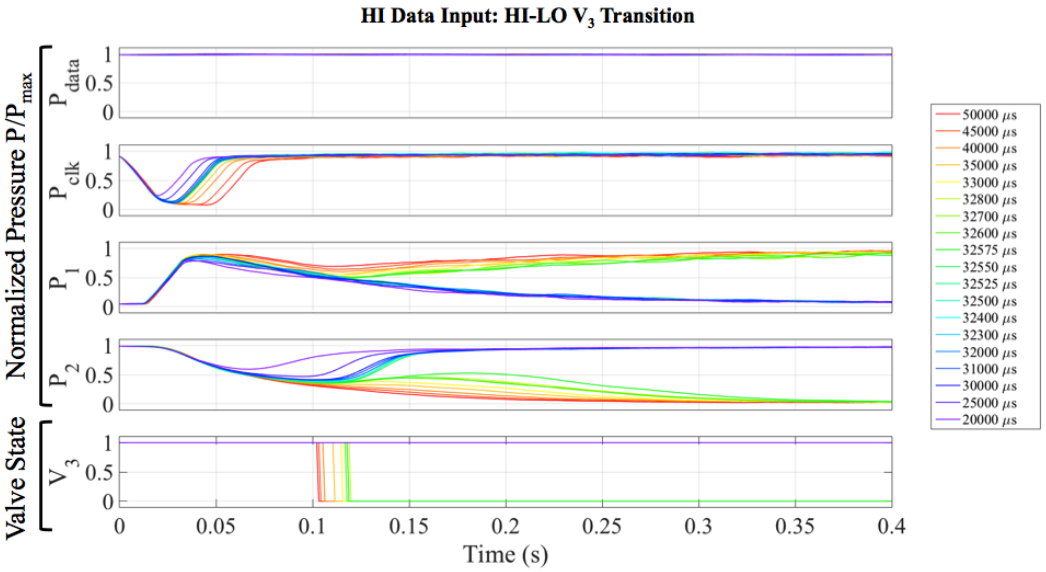

(a)

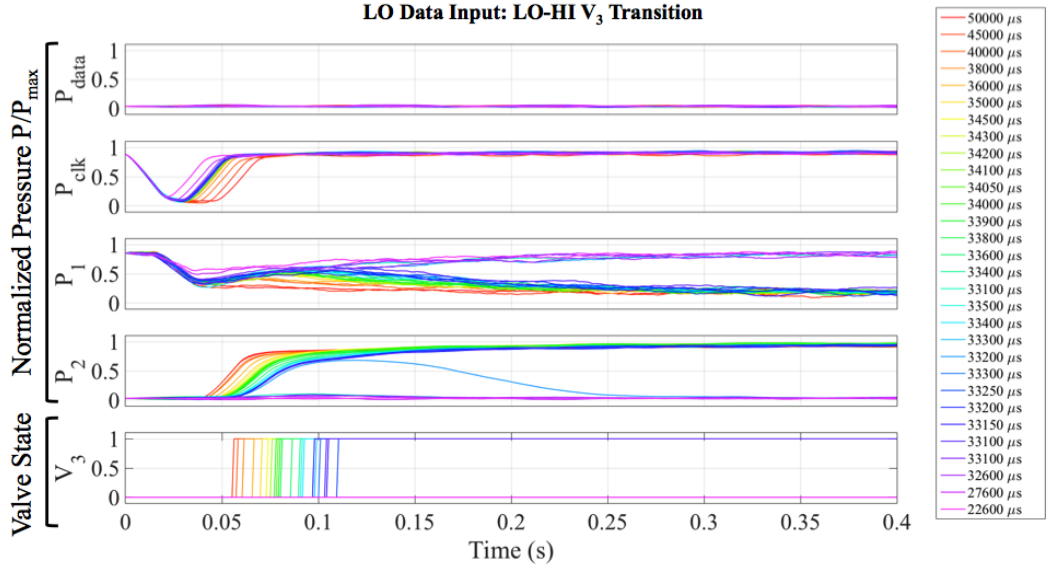

(b)

Figure 4.9: Results for the continuous-time pressures of the experimental D latch under different applied clock pulse widths. Two cases are presented for the D latch in which the inverted output is switched from (a) HI to LO and (b) LO to HI.

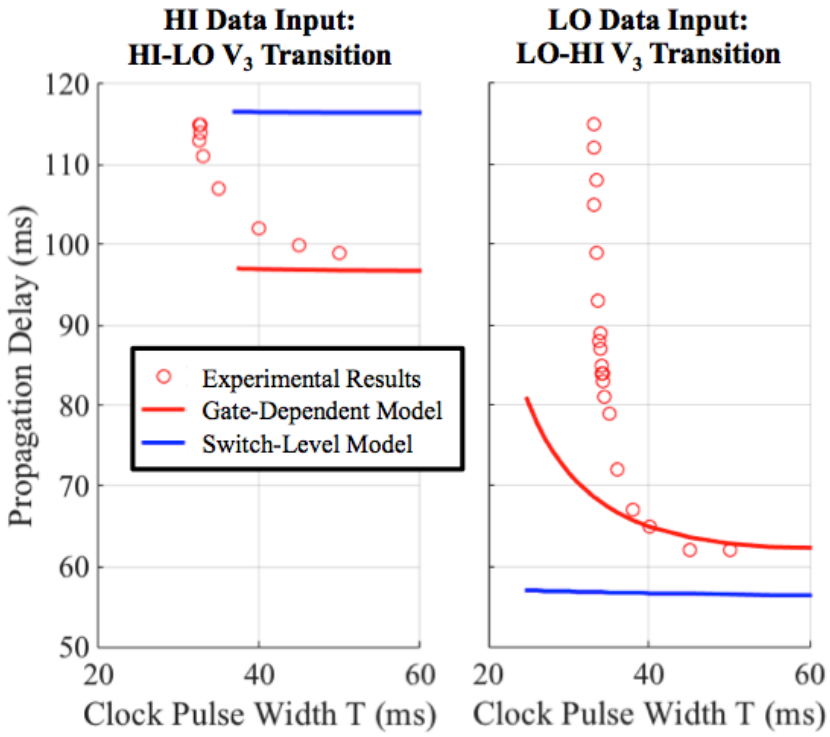

Figure 4.10: Experimental and simulation results for the propagation delays of the D latch for varying applied clock pulse widths. Two cases are presented for the D latch in which the inverted output is switched from HI to LO and LO to HI.

width is decreased for both HI-LO and LO-HI valid output transitions.

4.5 Discussion

The simulation of the hybrid automaton model outfitted with pressure-dependent valve resistance predicted a trend in the propagation delay for the LO-HI inverted output transition that is not predicted by switch-level model. This result is supported by derivations of metastable behavior in electronics in which propagation delay delay is directly related to the resistance and capacitance of circuit components and inversely related to the valve gain [42, p. 17]. For infinite valve gain, applied in the switch-level model, there is no change in propagation delay as input timing is changed. However, for the pressure-dependent valve resistance, valve gain varies with the gate pressure.

The simulation results for the LO-HI transition illustrate that the hybrid automaton model outfitted with the pressure-dependent valve model provides insight into input timing hazards not captured by typical switch-level modeling of the valves.

The simulation results for the HI-LO output transition did not predict any variation in propagation delay as clock pulse width was reduced. This result is consistent with using a perfect square wave for the clock input in simulation. The lack of rise time or fall time for the clock pulse results in a switch-level response of valve V_1. Therefore, only valves V_2 and V_3 would contribute to a difference in the D Latch response. Valve V_2 is initially in a closed configuration. The switch-level model and the gate-dependent model are identical in the closed configuration, so any difference in propagation delay between the two models would be from due to differences between the models when P_G is less than P_{op}. Referring to Fig. 4.8, there is minimal difference between the two models in this region. It is expected that there would be a constant propagation delay as clock pulse width is modulated for both models, which is in fact the case.

For the experimental D latch, the results showed a dependence of propagation delay on clock pulse width for the LO-HI transition that agrees with the simulation results of the hybrid automaton model described above. The approximated continuous-time traces (based on light reflection) for varying clock pulse widths are shown in Fig. 4.9. In the HI-LO experiment, there is a clear division between continuous-time traces for the flip-flop pressure output P_2 as the clock pulse width is decreases. At a certain point (light green in the Figure), the output pressure P_2 was not sufficient to open the subsequent valve gate (V_3 in Fig. 4.5). At that point, the flip-flop failed to change state and the clock pulse width was insufficient to cause a desired change in the flip-flop state based on the pressure input P_{data}. This point represents a "timing error", like that described by Grover et al. [22]. For the traces that eventually did drop to a low pressure, there is a clear difference in settling time that relates directly

to differences in the propagation delay shown in Fig. 4.10. A similar analysis of the LO-HI experiment leads to the same conclusion. As clock pulse width is increased, there are clear differences in the inverted pressure output P_2. At a point, the output pressure P_2 fails to go to a high pressure, due to an insufficient clock pulse width. The propagation delay is shown to increase as the clock pulse width increases until a "timing error" occurs, and the output does not reach the desired state based on the input P_{data}.

For the experimental D latch, the HI-LO propagation delay was found to be larger than the LO-HI propagation delay, which agrees with simulation of the hybrid automaton model. Additionally, the trend in the propagation delay that is characteristic of input timing changes in bistable circuits agrees with the simulated hybrid automaton model described above. The LO-HI and HI-LO propagation delays were about 60 ms and 100 ms, respectively, using clock pulse widths of approximately 50 ms. Therefore, the propagation delay for the experimental circuit dominated over the clock pulse width. The higher of the two propagation delays was 100 ms, which suggests a clock speed on the order of 10 Hz can be used in a sequential logic circuit using the experimental D latch elements.

The D latch design was implemented to produce an 8-dot braille cell that is controlled with just three electronic control valves. Fig. 4.11 shows a realization of the display that combines pneumatic actuators and pneumatic memory circuits. An 8-bit shift register (around the outside) built with 16 D latches in series addresses eight pneumatic actuators (in the center) that are arranged into a braille cell (dots 1.5 mm in diameter and 2.5 mm apart). The sequential D latches are addressed by alternating clock signals to form eight master-slave D flip-flops. The output of each D flip-flop addresses a pneumatic actuator in the center of the device. The device has been successfully controlled at 8 Hz, which is close to the 10 Hz predicted by propagation delay analysis of the D latch. We used standard microfabrication techniques to build

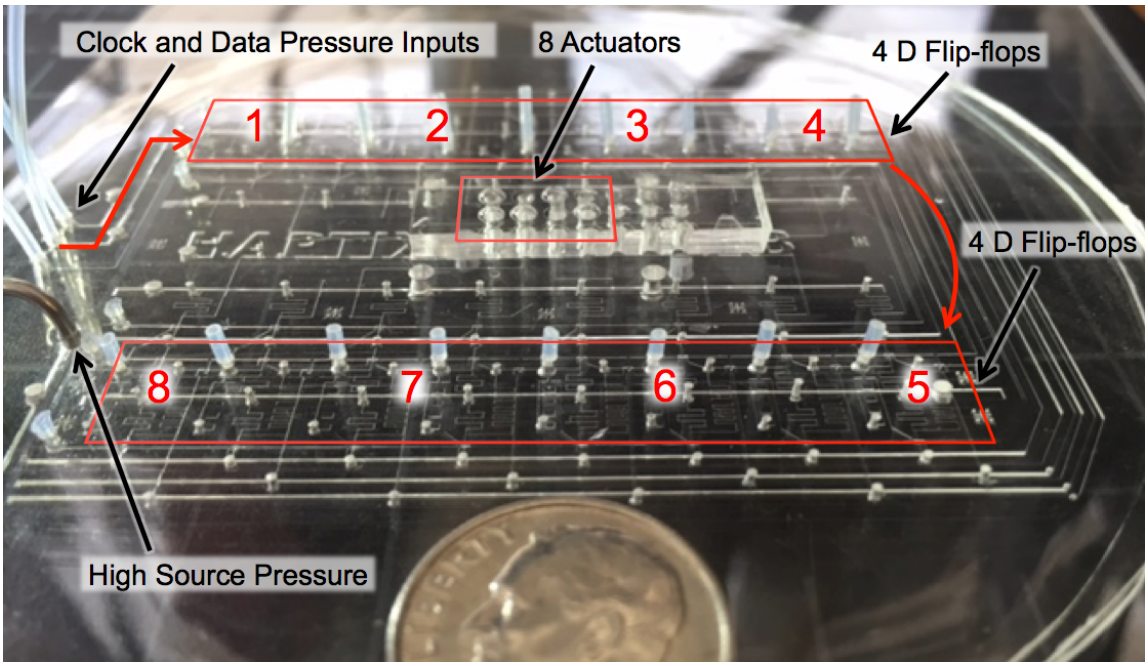

Figure 4.11: Pneumatic D latches are configured in series to create an 8-bit shift register that addresses an 8-dot braille cell. The actuators and addressing fluidic circuitry are batch-manufactured as a monolithic substrate using conventional microfabrication techniques.

the device, so the design can be easily scaled up with more actuators, making the technology suitable for creating a low-cost refreshable braille display.

4.6 Conclusions

This chapter presented a hybrid automaton model that contributes to understanding the clocking limits for pneumatic logic circuits. Duncan et al. detail the scaling of pneumatic resistance and capacitance of logic circuits to achieve lower propagation delays and thus higher operational speeds [16, 15]. The dependence of propagation delay on valve-specific behavior described in this chapter is not captured by the analytical model proposed by Duncan et al. or other models of pneumatic logic circuits in the microfluidics literature. Further, unlike previous work in characterizing circuit behavior of clock oscillators, the model presented in this chapter captures specific behavior characteristic of input-controlled bistable memory circuits. A shift regis-

ter uses sequential logic to enable control of an arbitrary number of pressure outputs (pneumatic actuators) with only two electronic pressure control inputs. One full clock cycle moves a bit of information along a shift register. The model presented herein contributes to characterizing the effect of valve behavior on the physical limit of information flow for pneumatic memory circuits that are essential for sequential logic operations. As such, the model represents a step toward more precise optimization of pneumatic memory circuits for improving response times and operational speeds in sequential logic operations.

CHAPTER V

Conclusions and Future Directions

A low-cost full-page tactile display would revolutionize the world of accessible braille products by providing blind people instant access to digital content at an affordable cost. However, the design of a display must consider perceptual limits related to braille reading while simultaneously overcoming the technical challenges associated with creating a dense array of refreshable dots. This dissertation presented a study that identified important factors in perceiving braille and developed models useful to the application of microfluidic technology for creating a refreshable braille display.

5.1 Contributions

1. **The Importance of Sliding Contact in Braille Letter Identification:** One design approach for refreshable braille is to reduce the number of actuators required by mounting a limited number of dots on movable substrate. The dots can be actuated according to the substrate motion to create the impression of pins that are tied to ground, when in fact the pins only move up and down with respect to the finger, not across it. In this dissertation, results from a perceptual study demonstrated that restricting sliding between the finger and dots significantly decreases performance in braille letter recognition.

2. **Relating Key Fluidic Valve Design Parameters to Cascadability of Fluidic Memory Circuits:** Implementing microfluidics for refreshable braille requires memory logic circuits that are cascadable. This dissertation presents a parameterized model that incorporates design elements common to fluidic valves in the literature to understand cascadable behavior. Results for valve membrane pre-load, effective stiffness, and resistance contribute to the development of a model that can serve as a valuable tool for understanding how design choices affect cascadable behavior.

3. **Relating Pressure-Dependent Resistance of Fluidic Valves to Fluidic Memory Circuit Timing:** Electronic braille displays require high refresh speeds. Prior work on the speed of fluidic circuits proposed for logic functions used switch-level models that did not consider continuous pressure-dependent behavior of fluidic valves. A fluidic valve model was developed and applied in the simulation of a D Latch memory circuit to reveal circuit timing behavior that had not been captured in previous models. The new model represents an improvement in understanding of micropneumatic memory circuits and is a step toward improving operation speeds of sequential logic circuits.

4. **Microfluidic Logic for Refreshable Braille** The application of microfluidic logic for controlling pneumatic actuators in a large-array tactile device has not been proposed previously. The experimental devices built in support of the modeling in the dissertation represent a step toward the creation of a large-array display using microfluidic technology. A refreshable braille cell was constructed in Chapter IV that relies on microfluidic logic to control eight actuators with only three electronic solenoid valves. While the device is larger than current commercial braille cells, it demonstrates the scalability of using microfluidic logic for a large-array of actuators suitable for refreshable braille.

5.2 Future Work

In this dissertation, significant contributions were made in the areas of (1) braille perception, specifically for the design of refreshable displays, and (2) the application of microfluidics for the creation of a braille displays. However, there are many more challenges and questions in those two areas that remain. The following subsections outline several potential areas for extending the work of this dissertation.

5.2.1 Perceptual Studies

In Chapter II, in addition to braille reading performance, we also collected motion tracking data to determine whether the various display and reading conditions would result in differences in micro-movements of the fingertips during reading. It is possible, for example, that readers compensated for the lack of lateral movement in static conditions by moving their finger laterally or vertically to increase stimulation of tactile receptors. It is also possible that readers employed small retrograde movements in the sliding conditions to 'check' the shape of symbols as the dot patterns passed beneath their fingertips. Analyzing the motion tracking data was initially unsuccessful, but a more rigorous experiment design might highlight the importance of these micro-movements in braille reading.

There are many larger questions which Chapter II raises. Firstly, it would be interesting to find a way to compare performance between non-proprioception and passive proprioception cases under conditions in which the user is entirely in control of their hand and arm movements. It would also be interesting to compare *static* and *sliding* conditions in a similar manner. Results might help determine whether, if cost is a factor, active control of a horizontally constrained single-cell display might be a viable low-cost alternative to a multi-cell refreshable braille line for displaying text content. An additional extension to the study in Chapter II would be to examine the effect of each display condition when reading spatially extended sequences of symbols

such as words (not just single braille characters).

Beyond thinking about the letters studied in Chapter II, it would be interesting to explore ways of displaying graphical content using larger arrays of actuated dots. Lateral motion and active proprioception are known to support the integration of tactile cues in haptic object exploration [38]. It is therefore likely that any display designed to render tactile graphics should preserve these cues. Findings further suggest that surface haptic displays which do not support fine featured traction distributions within the finger contact patch are likely to prove problematic for braille and tactile diagram interaction. It is an open question as to what role, if any, such displays can play in conveying meaningful information to blind computer users.

Fluidic actuator technology with addressing will lead to displays that can support braille and tactile graphical content in the same format. Future work might include studying active touch and human-device interaction made possible by the co-location of tactile features with user inputs. By increasing display refresh rates, it would be possible to design experiments in which inputs are co-located with tactile features and the user could actively control tactile content similar to the manner in which a sighted user interacts with a touchscreen.

5.2.2 Microfluidics for Refreshable Braille Displays

Chapter III and IV describe models that are useful for the design of cascaded pneumatic memory circuits. The experiments in Chapter III were done at a macroscale relative to the microscale valves described in the literature. A sweeping analysis of the valve model design parameters at a microscale has not yet been done. While the macroscale results are useful for understanding mechanistic reasons for valve behavior, future work could include a parallel parameter study on a family of microvalves. Chapter IV investigated the behavior of a single D Latch memory circuit under a full strength input signal. Future work could extend the model to cascaded bistable

circuits in which the output of one circuit is the input to the next. Circuit input signals would then depend on the the continuous-time pressures in previous circuits and would not necessarily be full strength. Additionally, the model described in Chapter IV may be useful in implementing dynamic logic, which is usually much faster than the typical static logic circuits employed in this dissertation and in the current microfluidics literature.

Chapter IV describes an eight-dot braille cell created by integrating microfluidic logic with pneumatic actuators. The underlying microfluidic circuitry needed to control the braille cell is about five times larger than is needed for creating a large-array refreshable braille device. Further, while the refresh rate for the single cell is sufficient, scaling up to more braille cells will require higher operational speeds. A typical full page of braille has 25 lines with up to 40 cells per line, where each cell consists of 8 braille dots (4x2). Therefore, a 100 by 80 grid of actuators (8000 total dots) would form a full-page RBD. Runyan cites that a refresh rate of 1 Hz is "tolerable" for a full-page display [55]. Therefore, given an X-Y addressable grid of pneumatic actuators and supporting D latches, if an electronic valve is used for each row and column, a propagation delay of 1 ms for each microfluidic D latch would result in a full-page refresh rate of 1 Hz. In this dissertation, a propagation delay of 100 ms was attained with a D latch test circuit. Devaraju et al. reported propagation delays of around 10 ms [14]. Further work on reducing the propagation delays for microfluidic logic circuits is therefore needed to achieve "tolerable" full-page refresh rates with microfluidic logic.

5.2.3 Microfluidics for New Shape Displays

A dense array of pneumatic actuators can potentially be used to implement a "taxelization" strategy. That is, a group of smaller tactile features can be raised together in a localized region to represent larger features that would be programmable in their

shape, size, and location. If integrated with a touch-sensing surface, such technology would enable the rendering of tactile environments using user input and system state. The device could cue specific tasks in time, or guide interaction dynamically with gravity wells and haptic tunnels to targets rendered on a surface. Real-time control of surface features would provide a rich palette of tactile cues available even when the finger is not moving. More importantly, perhaps, distinct cues are available within the finger contact patch. For example, a finger can be "nudged" in a programmable direction by actuating one or several bubbles adjacent to the finger's contact location. Also available might be radio buttons (depressing one button causes another to raise) or buttons that vibrate for attention. Virtual sliders formed from a line of bubbles might raise and lower under the finger, supporting path following and cuing knowledge of the current system state. The ability to render these tactile environments will open up new areas of research in surface haptics—areas that have previously been unavailable due to technological barriers.

BIBLIOGRAPHY

BIBLIOGRAPHY

[1] Hyperbraille: The project. URL `http://hyperbraille.de/project/`

[2] The Braille Literacy Crisis in America: Facing the Truth, Reversing the Trend, Empowering the Blind. Tech. Rep. 5, National Federation of the Blind Jernigan Institute (2009)

[3] Akbari, M., Sinton, D., Bahrami, M.: Pressure Drop in Rectangular Microchannels as Compared With Theory Based on Arbitrary Cross Section. Journal of Fluids Engineering **131**(4), 041,202 (2009). DOI 10.1115/1.3077143

[4] Bar-Cohen, Y.: Refreshable Braille displays using EAP actuators. In: Y. Bar-Cohen (ed.) SPIE Smart Structures and Materials + Nondestructive Evaluation and Health Monitoring, pp. 764,206–764,206–5. International Society for Optics and Photonics (2010). DOI 10.1117/12.844698

[5] Bau, O., Poupyrev, I., Israr, A., Harrison, C.: TeslaTouch : Electrovibration for Touch Surfaces. In: Proceedings of the 23nd annual ACM symposium on User interface software and technology, {UIST} '10, pp. 283–292. ACM, New York, NY (2010). DOI 10.1145/1866029.1866074

[6] Benali-Khoudja, M., Hafez, M., Alexandre, J.M., Kheddar, A.: Tactile interfaces: a state-of-the-art survey. In: Int. Symposium on Robotics, vol. 31, pp. 23–26. Citeseer (2004)

[7] Brody, T., Szepesi, Z., Davies, D.: A 6 x 6-in 20-lpi electroluminescent display panel. IEEE Transactions on Electron Devices **22**(9), 739–748 (1975). DOI 10.1109/T-ED.1975.18214

[8] Brown, G.G.: Means of communication with the blind (1916)

[9] Bryce, J.: Reading apparatus (1950)

[10] Bürklen, K.: Touch reading of the blind, 1932 trans edn. American Foundation for the Blind, New York (1932)

[11] Chen, H., Gu, W., Cellar, N., Kennedy, R., Takayama, S., Meiners, J.C.: Electromechanical properties of pressure-actuated PDMS microfluidic push-down valves. Analytical chemistry **80**(15), 6110 (2008)

[12] Cheow, L.F., Yobas, L., Kwong, D.L.: Digital microfluidics: Droplet based logic gates. Applied Physics Letters **90**(5), 54,103–54,107 (2007). DOI doi:10.1063/1.2435607

[13] Chubb, E.C., Colgate, J.E., Peshkin, M.A.: ShiverPaD: A Glass Haptic Surface That Produces Shear Force on a Bare Finger. IEEE Transactions on Haptics **3**(3), 189–198 (2010). DOI 10.1109/TOH.2010.7

[14] Devaraju, N.S.G.K., Unger, M.A.: Pressure driven digital logic in PDMS based microfluidic devices fabricated by multilayer soft lithography. Lab on a chip **12**(22), 4809–15 (2012). DOI 10.1039/c2lc21155f

[15] Duncan, P.N., Ahrar, S., Hui, E.E.: Scaling of pneumatic digital logic circuits. Lab Chip **15**(5), 1360–1365 (2015). DOI 10.1039/C4LC01048E

[16] Duncan, P.N., Nguyen, T.V., Hui, E.E.: Pneumatic oscillator circuits for timing and control of integrated microfluidics. Proceedings of the National Academy of Sciences of the United States of America **110**(45), 18,104–9 (2013). DOI 10.1073/pnas.1310254110

[17] Foley, C.: Characterizing metastability. In: Proceedings Second International Symposium on Advanced Research in Asynchronous Circuits and Systems, p. /8. IEEE Comput. Soc. Press (1996). DOI 10.1109/ASYNC.1996.494449

[18] Fordyce, P.M., Diaz-Botia, C.A., DeRisi, J.L., Gomez-Sjoberg, R.: Systematic characterization of feature dimensions and closing pressures for microfluidic valves produced via photoresist reflow. Lab on a chip **12**(21), 4287–95 (2012). DOI 10.1039/c2lc40414a

[19] Foulke, E., Schiff, W. (eds.): Tactual Perception: a sourcebook. Cambridge University Press, New York (1982)

[20] Gibson, J.J.: Observations on active touch. Psychological Review **69**(6), 477–91 (1962)

[21] Gibson, J.J.: The senses considered as perceptual systems. Houghton Mifflin, Boston (1966)

[22] Grover, W.H., Ivester, R.H.C., Jensen, E.C., Mathies, R.A.: Development and multiplexed control of latching pneumatic valves using microfluidic logical structures. Lab on a chip **6**(5), 623–631 (2006). DOI 10.1039/b518362f

[23] Grover, W.H., Skelley, A.M., Liu, C.N., Lagally, E.T., Mathies, R.A.: Monolithic membrane valves and diaphragm pumps for practical large-scale integration into glass microfluidic devices. Sensors and Actuators B: Chemical **89**(3), 315–323 (2003). DOI 10.1016/S0925-4005(02)00468-9

[24] Grunwald, A.P.: Reading and writing machine using raised patterns (1971)

[25] Heller, M.: Active and passive tactile braille recognition. Bulletin of the psychonomic society **24**(3), 201–202 (1986)

[26] Heller, M.a.: Tactile picture perception in sighted and blind people. Behavioural brain research **135**(1-2), 65–8 (2002)

[27] Hislop, D.W., Zuber, B.L., Trimble, J.L.: Text-scanning patterns of blind readers using Optacon and braille. Journal of rehabilitation research and development **22**(3), 54–65 (1985)

[28] Hosokawa, K., Maeda, R.: Low-cost technology for high-density microvalve arrays using polydimethylsiloxane (PDMS). In: Technical Digest. MEMS 2001. 14th IEEE International Conference on Micro Electro Mechanical Systems (Cat. No.01CH37090), pp. 531–534. IEEE. DOI 10.1109/MEMSYS.2001.906596

[29] Hosokawa, K., Maeda, R.: A pneumatically-actuated three-way microvalve fabricated with polydimethylsiloxane using the membrane transfer technique. Journal of Micromechanics and Microengineering **10**(3), 415–420 (2000). DOI 10.1088/0960-1317/10/3/317

[30] Jensen, E.C., Grover, W.H., Mathies, R.A.: Micropneumatic Digital Logic Structures for Integrated Microdevice Computation and Control. Journal of Microelectromechanical Systems **16**(6), 1378–1385 (2007). DOI 10.1109/JMEMS.2007.906080

[31] Johansson, R.S., Westling, G.: Roles of glabrous skin receptors and sensorimotor memory in automatic control of precision grip when lifting rougher or more slippery objects. Experimental Brain Research **56**(3), 550–564 (1984). DOI 10.1007/BF00237997

[32] Juan-Chico, J., Bellido, M.J., Acosta, A.J., Valencia, M., Huertas, J.L.: Analysis of metastable operation in a cmos dynamic d-latch. In: Analog Design Issues in Digital VLSI Circuits and Systems, pp. 143–157. Springer (1997)

[33] Kartalov, E.P., Scherer, A., Quake, S.R., Taylor, C.R., Anderson, W.F.: Experimentally validated quantitative linear model for the device physics of elastomeric microfluidic valves. Journal of Applied Physics **101**(6), 064,505 (2007). DOI 10.1063/1.2511688

[34] Katz, D.: Der Aufbau der Tastwelt: Zeitschrift fUr Psychologie Ergänzungsband 11. Zeitschrift fUr Psychologie, Leipzig (1925)

[35] Kleeman, L., Cantoni, A.: Metastable behavior in digital systems. IEEE Design & Test of Computers **4**(6), 4–19 (1987)

[36] Krueger, L.E.: A word-superiority effect with print and braille characters. Perception & Psychophysics **31**(4), 345–352 (1982). DOI 10.3758/BF03202658

[37] Kyung, K.u.K., Kim, S.: Texture Display Mouse KAT : Vibrotactile Pattern and Roughness Display. Intelligent Robots and ... pp. 478–483 (2006)

[38] Lederman, S.J., Klatzky, R.L.: Hand movements: A window into haptic object recognition. Cognitive Psychology **19**(3), 342–368 (1987). DOI 10.1016/0010-0285(87)90008-9

[39] Legge, G.G., Madison, C., Mansfield, J.: Measuring Braille reading speed with the MNREAD test. Visual impairment research **1**(3), 131–145 (1999). DOI 10.1076/vimr.1.3.131.4438

[40] Loomis, J.M.: On the tangibility of letters and braille. Perception & Psychophysics **29**(1), 37–46 (1981). DOI 10.3758/BF03198838

[41] Marino, L.R.: General theory of metastable operation. IEEE Transactions on Computers **100**(2), 107–115 (1981)

[42] Melchiorre, R.: A study of metastability in CMOS latches (1992)

[43] Millar, S.: Reading by Touch. Routledge, London (1997)

[44] Mohan, R., Schudel, B.R., Desai, A.V., Yearsley, J.D., Apblett, C.A., Kenis, P.J.: Design considerations for elastomeric normally closed microfluidic valves. Sensors and Actuators B: Chemical **160**(1), 1216–1223 (2011). DOI 10.1016/j.snb.2011.09.051

[45] Mosadegh, B., Kuo, C.H., Tung, Y.C., Torisawa, Y.S., Bersano-Begey, T., Tavana, H., Takayama, S.: Integrated Elastomeric Components for Autonomous Regulation of Sequential and Oscillatory Flow Switching in Microfluidic Devices. Nature physics **6**(6), 433–437 (2010). DOI 10.1038/nphys1637

[46] Mosadegh, B., Tavana, H., Lesher-Perez, S.C., Takayama, S.: High-density fabrication of normally closed microfluidic valves by patterned deactivation of oxidized polydimethylsiloxane. Lab on a chip **11**(4), 738–42 (2011). DOI 10.1039/c0lc00112k

[47] Munson, B.R., Young, D.F., Okiishi, T.H., Huebsch, W.H.: Fundamentals of Fluid Mechanics. John Wiley & Sons, Inc. (2009)

[48] Nolan, C.Y., Kederis, C.J.: Perceptual factors in braille word recognition. American Foundation for the Blind, Louisville (1969)

[49] Ogata, K.: System Dynamics. 4th

[50] Prakash, M., Gershenfeld, N.: Microfluidic Bubble Logic. Science **315**(5813), 832–835 (2007). DOI 10.1126/science.1136907

[51] Rhee, M., Burns, M.A.: Microfluidic pneumatic logic circuits and digital pneumatic microprocessors for integrated microfluidic systems. Lab on a Chip **9**(21), 3131–3143 (2009). DOI 10.1039/B904354C

[52] Richard, E., Feinman, A.M., Wottawa, C., Chih-Hung, K., Franco, M.L., Dutson, E.P., Grundfest, W.S., Culjat, M.O.: Characterization of a pneumatic balloon actuator for use in refreshable Braille displays. Medicine Meets Virtual Reality Seventeen **142**, 94 (2009)

[53] Robles-De-La-Torre, G., Hayward, V.: Force can overcome object geometry in the perception of shape through active touch. Nature **412**(6845), 445–8 (2001). DOI 10.1038/35086588

[54] Runyan, N., Blazie, D.: EAP actuators aid the quest for the 'Holy Braille' of tactile displays. In: Y. Bar-Cohen (ed.) Electroactive Polymer Actuators and Devices, pp. 764,207–1 – 764,207–12. International Society for Optics and Photonics (2010). DOI 10.1117/12.847764

[55] Runyan, N.H., Blazie, D.B.: The continuing quest for the 'Holy Braille' of tactile displays. In: J. Esteve, E.M. Terentjev, E.M. Campo (eds.) SPIE NanoScience + Engineering, vol. 8107, pp. 81,070G–81,070G–17. International Society for Optics and Photonics (2011). DOI 10.1117/12.897382

[56] Runyan, N.H., Carpi, F.: Seeking the holy braille' display: might electromechanically active polymers be the solution? Expert review of medical devices **8**(5), 529–532 (2011)

[57] Russomanno, A., Gillespie, R.B., O'Modhrain, S., Barber, J.: A tactile display using pneumatic membrane actuators. In: Eurohaptics proceedings, pp. 445–447 (2014)

[58] Russomanno, A., Gillespie, R.B., O'Modhrain, S., Barber, J.: Modeling Pneumatic Actuators for a Refreshable Tactile Display. In: Eurohaptics proceedings, pp. 385–393 (2014)

[59] Russomanno, A., Gillespie, R.B., O'Modhrain, S., Burns, M.: The design of pressure-controlled valves for a refreshable tactile display. In: World Haptics Conference (WHC), 2015 IEEE, pp. 177–182 (2015). DOI 10.1109/WHC.2015.7177710

[60] Russomanno, A., O'Modhrain, S., Gillespie, R.B., Rodger, M.: Refreshing Refreshable Braille Displays. Transactions on Haptics (2015)

[61] Schomburg, W.K.: Membranes. Introduction to Microsystem Design pp. 191–201 (2011). DOI 10.1007/978-3-642-19489-4

[62] Studer, V.: Scaling properties of a low-actuation pressure microfluidic valve. Journal of Applied Physics **95**(1), 393 (2004). DOI 10.1063/1.1629781

[63] Takao, H., Ishida, M.: Microfluidic integrated circuits for signal processing using analogous relationship between pneumatic microvalve and MOSFET. Journal of Microelectromechanical Systems **12**(4), 497–505 (2003). DOI 10.1109/JMEMS.2003.815838

[64] Takao, H., Ishida, M., Sawada, K.: A pneumatically actuated full in-channel microvalve with MOSFET-like function in fluid channel networks. Journal of Microelectromechanical Systems **11**(5), 421–426 (2002). DOI 10.1109/JMEMS.2002.803414

[65] Takao, H., Miyamura, K., Ebi, H., Ashiki, M., Sawada, K., Ishida, M.: A MEMS microvalve with PDMS diaphragm and two-chamber configuration of thermo-pneumatic actuator for integrated blood test system on silicon. Sensors and Actuators A: Physical **119**(2), 468–475 (2005)

[66] Thorsen, T., Maerkl, S.J., Quake, S.R., Hadd, A.G., Jacobson, S.C., Ramsey, J.M., Harrison, D.J., Li, P.C.H., Harrison, D.J., Hadd, A.G., Raymond, D.E., Haliwell, J.W., Jacobson, S.C., Ramsey, S.C., Lagally, E.T., Medintz, I., Mathies, R.A., Khandurina, J., Eteshola, E., Leckband, D., Wang, J., Ibanez, A., Chatrathi, M.P., Escarpa, A., Unger, M.A., Chou, H.P.P., Thorsen, T., Scherer, A., Quake, S.R., Buchaillot, L., Farnault, E., Hoummady, M., Fujita, H., Chou, H.P.P., Spence, C.S., Scherer, A., Quake, S.R., Linder, V., Verpoorte, E., Thormann, W., de Rooij, N.F., Sigrist, H., Yang, T., Jung, S., Mao, H., Cremer, P.S., Duffy, D.C., MacDonald, J.C., Schueller, O.J.A., Whitesides, G.M., Grzybowski, B.A., Haag, R., Bowden, N., Whitesides, G.M.: Microfluidic large-scale integration. Science (New York, N.Y.) **298**(5593), 580–4 (2002). DOI 10.1126/science.1076996

[67] Tong, J., Mao, O., Goldreich, D.: Two-point orientation discrimination versus the traditional two-point test for tactile spatial acuity assessment. Frontiers in Human Neuroscience **7**(September), 579 (2013). DOI 10.3389/fnhum.2013.00579

[68] Unger, M.A.: Monolithic Microfabricated Valves and Pumps by Multilayer Soft Lithography. Science **288**(5463), 113–116 (2000). DOI 10.1126/science.288.5463.113

[69] Van Der Schaft, A.J., Schumacher, J.M.: An introduction to hybrid dynamical systems, vol. 251. Springer-Verlag London (2000)

[70] Varao Sousa, T.L., Carriere, J.S.a., Smilek, D.: The way we encounter reading material influences how frequently we mind wander. Frontiers in psychology **4**(November), 892 (2013). DOI 10.3389/fpsyg.2013.00892

[71] Vestad, T., Marr, D.W.M., Munakata, T.: Flow resistance for microfluidic logic operations. Applied Physics Letters **84**(25), 5074–5075 (2004). DOI doi:10.1063/1.1764592

[72] Vidal-Verdú, F., Hafez, M., Vidal-Verdu, F., Hafez, M., Vidal-Verdú, F., Hafez, M.: Graphical tactile displays for visually-impaired people. IEEE transactions on neural systems and rehabilitation engineering : a publication of the IEEE Engineering in Medicine and Biology Society **15**(1), 119–130 (2007). DOI 10.1109/TNSRE.2007.891375

[73] Vitello, M.P., Fritschi, M., Ernst, M.O.: Active Movement Reduces the Tactile Discrimination Performance. In: A. Peer, C.D. Giachritsis (eds.) Immersive Multimodal Interactive Presence, Springer Series on Touch and Haptic Systems, chap. 2, pp. 7–34. Springer London, London (2012). DOI 10.1007/978-1-4471-2754-3

[74] Ward, S.A., Halstead, R.H.: Computation Structures (1991)

[75] Weathers, T.M.: NASA contributions to fluidic systems: A survey (1972)

[76] Weaver, J.A., Melin, J., Stark, D., Quake, S.R., Horowitz, M.A.: Static control logic for microfluidic devices using pressure-gain valves. Nature Physics **6**(3), 218–223 (2010). DOI 10.1038/nphys1513

[77] Winfield, L., Glassmire, J., Colgate, J.E., Peshkin, M.: T-PaD: Tactile Pattern Display through Variable Friction Reduction. In: Second Joint EuroHaptics Conference and Symposium on Haptic Interfaces for Virtual Environment and Teleoperator Systems (WHC'07), pp. 421–426. IEEE (2007). DOI 10.1109/WHC.2007.105

[78] Wu, X., Zhu, H., Kim, S.H., Allen, M.G.: A Portable Pneumatically-Actuated Refreshable Braille Cell. In: TRANSDUCERS 2007 - 2007 International Solid-State Sensors, Actuators and Microsystems Conference, pp. 1409–1412. IEEE (2007). DOI 10.1109/SENSOR.2007.4300407

[79] Xu, C., Israr, A., Poupyrev, I., Bau, O., Harrison, C.: Tactile display for the visually impaired using TeslaTouch. In: CHI'11 Extended Abstracts on Human Factors in Computing Systems, pp. 317–322. ACM, ACM Press, New York, New York, USA (2011). DOI 10.1145/1979742.1979705

[80] Yobas, L., Durand, D., Skebe, G., Lisy, F., Huff, M.: A novel integrable microvalve for refreshable braille display system. Journal of Microelectromechanical Systems **12**(3), 252–263 (2003). DOI 10.1109/JMEMS.2003.811754